ARTICLE

Solution-Phase Synthesis of Group 3-5 Transition Metal Chalcogenide Inorganic Nanomaterials

Received 00th January 20xx,
Accepted 00th January 20xx

DOI: 10.1039/x0xx00000x

Daniel Zilevu[a] and Sidney E. Creutz*[a]

The versatility of early transition metal chalcogenide nanomaterials, including chalcogenide perovskites, has attracted enormous attention for a variety of applications, such as photovoltaics, photocatalysis, and optoelectronic devices. These nanomaterials exhibit unique electronic and optical properties, allowing for a broad range of applications, depending on their chemical composition and crystal structure. However, solution-phase synthesis of early transition metal chalcogenide nanocrystals is challenging due, in part, to their high crystallization energy and oxophilicity. In this feature article, we explore various synthetic routes reported for inorganic ternary and binary sulfide and selenide nanomaterials that include transition metals from groups 3, 4, and 5. By systematically comparing different synthetic approaches, we identify trends and insights into the chemistry of these chalcogenide nanomaterials.

Introduction

The continuous search for new inorganic semiconductor materials to fulfil critical roles in energy storage and conversion—including as thin-film photovoltaic absorbers, catalysts, and battery materials—has led increasingly to the prediction and attempted realization of material compositions combining ions from disparate parts of the periodic table and with widely varying chemical properties. As an example that represents a major motivation for this article, ternary $(AE)M^{4+}Q_3$ materials, where AE = alkaline earth metal, M^{4+} is a group 4 transition metal cation, and Q is a chalcogenide (sulfide or selenide), have recently drawn focus because some members of this class, especially the distorted perovskite material $BaZrS_3$, have significant potential as absorbers for thin-film solar cells, or possibly in other optoelectronic devices.[1] In part because of the difficulty of generating high-quality thin films of these materials at reasonable temperatures, there has been considerable interest in preparing these materials as colloidal nanocrystals which could be used as inks for solution processing of thin films. Colloidal nanomaterials of these ternary early transition metal chalcogenides have only recently been realized, and considerable room for optimization remains.[2–4]

Part of the challenge in the low-temperature synthesis of nanomaterials such as $BaZrS_3$ may lie in the combination of an oxophilic early transition metal cation (Zr^{4+}) with a soft chalcogenide anion (S^{2-}), a pairing that would traditionally be considered unfavorable. In general, there is a paucity of reported synthetic routes to early transition metal chalcogenide nanomaterials, including both ternary materials such as $BaZrS_3$ and binary materials such as TiS_2 and ZrS_2. While the ternary $(AE)M^{4+}Q_3$ materials, and other examples of ternary materials in this class such as the sulvanites ($Cu_3M'S_4$, M' = V, Nb, Ta), are of interest because of their potential optoelectronic applications including in solar cells, many of the binary materials boast layered structures that make them of interest for battery materials, and many also may have (photo)catalytic applications.[5–13]

While the preparation of phase-pure ternary materials presents special challenges given the need to balance the reactivity of different metal precursors, important lessons can be learned from understanding the synthetic pathways and approaches to the related binary materials. The goal of this feature article, therefore, is to interrogate this area to develop an understanding of the current state-of-the-art of early transition metal chalcogenide nanomaterial synthesis, including both ternary and binary materials. A number of the binary nanomaterials discussed here fall into the general category of two-dimensional transition metal dichalcogenides, and have been discussed in that context in other recent reviews.[14–16]

The bulk of this article consists of a comprehensive survey of reported synthetic routes to ternary and binary sulfide and selenide nanomaterials which include transition metals from groups 3, 4, and 5. During the course of this survey, we will highlight major trends and contrasts both within and among different materials. Our own work on the synthesis of chalcogenide perovskites and related nanomaterials ($BaTiS_3$ and $BaZrS_3$) is highlighted, and we discuss some of the remaining unknowns about the synthesis and properties of these materials. After this survey, we attempt to summarize general trends that have emerged in the synthetic methodologies to date, and suggest specific areas where further development of precursors, solvents, ligands, and reaction conditions is needed. This discussion will emphasize the chemical differences between early transition metals and

[a] Department of Chemistry, Mississippi State University, Mississippi State, MS 39762. E-mail: screutz@chemistry.msstate.edu

late transition metals or p-block metals which must be taken into account when developing new methodologies for their synthesis.

The discussion in this article is focused on reports where nanomaterials are produced by a "bottom-up" route from solution-phase precursors, rather than "top-down" synthetic routes involving, for example, exfoliation of bulk crystals. Additionally, we emphasize reports where the products are discrete nanoparticles rather than thin films, larger microcrystals, or bulk materials. However, key examples of top-down synthetic routes to colloidal nanomaterials, and of the solution-phase preparation of thin films, are briefly discussed in some cases where they provide important context, especially for materials where few or no examples of solution-phase colloidal nanocrystal syntheses are yet known.

The solution-phase synthetic methods described in the discussion here are also summarized comparatively in a detailed table in the Supplementary Information (Table S1).

Synthesis of Early Transition Metal Chalcogenide Nanomaterials

Group 3 Transition Metal Chalcogenide Nanomaterials

There are currently no published examples of solution-synthesized colloidal nanomaterials of binary or ternary scandium chalcogenides, and only one example of an yttrium chalcogenide nanomaterial, $NaYS_2$. Detailed discussion of the other rare earth elements La – Lu is omitted here, although in their trivalent forms these ions share many chemical properties with Sc^{3+} and Y^{3+}, and are likewise relatively difficult to prepare as chalcogenides, especially for the later members of the series. However, it is worth noting that a number of examples of the preparation of trivalent lanthanide sulfide and selenide colloidal nanomaterials have been reported in recent years.[17–19]

The solution-phase preparation of $NaYS_2$ nanocrystals (Figure 1) was reported in 2012 by Zhang and Yan as part of a series that also included the preparation of $NaLnS_2$ nanomaterials (Ln = all lanthanides except Pm).[20] By combining yttrium(III) acetylacetonate, sodium oleate, and excess H_2S (supplied as a gas) in hexadecylamine (HDA) and octadecene (ODE) at 280 °C, they were able to produce $NaYS_2$ nanohexagons roughly 50-100 nm in size.

In what they termed a "chemoaffinity-mediated" synthesis, the authors found that by incorporating sodium ions into their synthesis in excess, in combination with H_2S as a reactive sulfur source, they could favor the formation of a sulfide material

Figure 1. Synthesis of $NaYS_2$ nanocrystals and TEM image of the resulting particles (A), reprinted with permission from Y. Ding, J. Gu, T. Zhang, A.-X. Yin, L. Yang, Y.-W. Zhang, and C.-H. Yan. *J. Am. Chem. Soc.* 2012, **134**, 3255-3264. Copyright 2012 American Chemical Society.

(such as $NaYS_2$) rather than oxysulfides or oxides, despite the fact that oxygen-containing precursors (acetylacetonates and oleates) were used. Unfortunately, binary sulfides (e.g. Y_2S_3) most likely could not be formed using this method; in the case of $NaLaS_2$, which was the most thoroughly studied of the materials reported, omission of the Na(acac) precursor (or the use of less equivalents) resulted in partial or complete formation of oxysulfides instead of the desired product.

Binary Group 4 Transition Metal Chalcogenide Nanomaterials

Known binary group 4 transition metal chalcogenide nanomaterials prepared by solution synthesis include most prominently TiS_2 and ZrS_2, while more limited examples of HfS_2, $TiSe_2$, $ZrSe_3$, and $HfSe_3$ are known; all of these have 2-D layered structures and are formed with nanoplatelet or nanosheet morphologies, controllable in some cases down to single layers.[21]

Binary Titanium Chalcogenides. Colloidal syntheses of TiS_2 (Figure 2) were first reported in 2008 using a heat-up approach[22,23] by the Son group, who combined elemental sulfur in oleylamine (OlAm) with $TiCl_4$ in oleylamine to give an initially blue-black solution, which, upon heating for 12 hours at 215 °C, gave rise to colloidal single-layer nanodiscs of controllable lateral sizes (Figure 2A).[24] Later, Plashnitsa *et al.* used the same precursors under modified conditions (300 °C for 3 hours) to produce large multilayer TiS_2 nanosheets (Figure 2C).[25] $TiCl_4$, which is a liquid at room temperature and forms an unidentified orange precipitate upon addition to oleylamine,[24] has been used as the titanium precursor in practically all published syntheses of TiS_2 and $TiSe_2$ nanomaterials. Oleylamine is nearly ubiquitous as the solvent of choice, although Plashnitsa reported that TiS_2 materials could also be formed using other amine solvents (dodecylamine and hexadecylamine, which gave rise to nanorods), the alkane solvent squalane (which produced nanoparticles), and even trioctylphosphine oxide (which gave rise to an uncontrolled assortment of morphologies); however, complete characterization data for the materials from these reactions was not provided.[20] In another example of solvent variation, Tilley *et al.* prepared nanoflowers and nanoflakes of TiS_2 by hot-injection[23,26] of $TiCl_4$ at different temperatures into a sulfur-octadecene solution; however, given the lack of stabilizing ligands, the resulting materials formed as insoluble powders rather than colloids (Figure 2B).[27] Later, by altering the solvent mixture to oleylamine and oleic acid (in a 7:1 ratio), they were able to isolate inorganic fullerene (IF) nanoparticles and hollow IF nanospheres of TiS_2, when either a hot-injection (injection of $TiCl_4$ at 250 °C followed by raising the temperature to 300 °C) or heat-up (from room temperature to 300 °C) approach was used, respectively.[28] Elemental analysis data (EDS) confirmed the purity of the material, with minimal oxide contamination.

Variations in the sulfur precursor have been explored in order to tune the quality and properties of the resulting TiS_2 nanomaterials. In particular, the Cheon group found that using CS_2 (*via* hot-injection) as the sulfur precursor—forming a dithiocarbamate species *in situ* by reaction with oleylamine—gave rise to higher-quality TiS_2 nanodiscs, in terms of

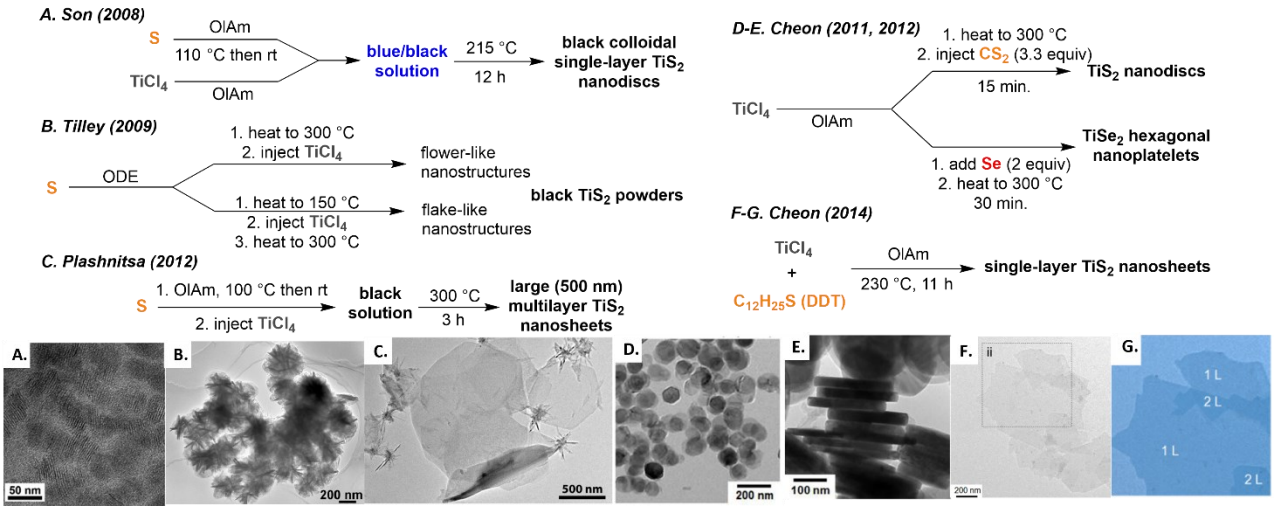

Figure 2. Syntheses of TiS_2 and $TiSe_2$ nanomaterials. (A) Synthesis of TiS_2 nanodiscs that self-assemble into stacks, as shown in the TEM image. Adapted from ref. 24 with permission, Copyright © 2008 Wiley-VCH Verlag GmbH & Co. KGaA, Weinheim. (B) Synthesis of nanostructured TiS_2 materials using hot injection of $TiCl_4$ at different temperatures; TEM image shows outcome from injection at 300 °C. Adapted with permission from S. Prabakar, C. W. Bumby, R. D. Tilley. *Chem. Mater.* 2009, **21**, 1725-1730. Copyright 2009 American Chemical Society. (C) Preparation of large-area TiS_2 nanosheets. Adapted with permission from V. V. Plashnitsa, F. VIetmeyer, N. Petchsang, P. Tongying, T. H. Kosel, and M. Kuno. *J. Phys. Chem. Lett.* 2012, 1554-1558. Copyright 2012 American Chemical Society. (D-E) Hot-injection synthesis of TiS_2 nanodiscs (D) and heat-up synthesis of $TiSe_2$ nanoplatelets (E), adapted with permission from S. Jeong, D. Yoo, J. Jang, M. Kim, and J. Cheon. *J. Am. Chem. Soc.* 2012, **134**, 18233-18236. Copyright 2012 American Chemical Society. (F-G) Single-layer TiS_2 nanosheets, showing TEM image (F) and pseudocolor image (G) for boxed area; scale bar is 200 nm. Adapted with permission from D. Yoo, M. Kim, S. Jeong, J. Han, and J. Cheon. *J. Am. Chem. Soc.* 2014, **136**, 14670-14673. Copyright 2014 American Chemical Society.

crystallinity and uniformity, as compared to using elemental sulfur under otherwise similar conditions (Figure 2D).[29,30] They attributed this to the fact that the reaction and subsequent decomposition of CS_2 formally generates H_2S in situ without the involvement of radical intermediates, whereas the dissolution of sulfur in oleylamine generates sulfur radicals, which they observed by EPR. Deleterious and uncontrolled reactions with these sulfur radicals were proposed to be the reason for the lower quality of the nanocrystals produced from elemental sulfur. Notably, this approach using CS_2 injection could also be extended to the other group 4 transition metal sulfides (ZrS_2 and HfS_2, *vide infra*).[29]

The Cheon group further elaborated on this synthetic approach by using 1-dodecanethiol (DDT) as the sulfur source (formally *via* H_2S formed during the *in situ* decomposition of this precursor), which gave rise to the controlled production of high-quality single-layer TiS_2 nanosheets (Figure 2F-G). Again, the same approach could be used for ZrS_2 and HfS_2, and the details of this process are discussed further below.[21]

Reports of the solution-phase colloidal $TiSe_2$ nanomaterials are scarce, with the only published example also from the Cheon group (Figure 2E).[29] Combining elemental selenium with $TiCl_4$ in oleylamine *via* a heat-up protocol at 300 °C gave rise to large (~250 nm diameter) $TiSe_2$ nanoplatelets with a well-defined hexagonal shape. It was hypothesized that although selenium radicals were formed during the dissolution of selenium in oleylamine, they were less reactive than the similarly formed sulfur radicals, and therefore were less detrimental to the formation of high-quality nanocrystals.

Binary Zirconium Chalcogenides. Cheon *et al.* have reported the only well-characterized examples of the solution-phase synthesis of colloidal ZrS_2 and $ZrSe_3$ nanomaterials, which were prepared by methods analogous to those described above for TiS_2, using $ZrCl_4$ as the metal precursor and oleylamine as the solvent. Hot injection of CS_2 into $ZrCl_4$ in oleylamine at 300 °C gave rise to uniform three-layer nanodiscs whose lateral size could be controlled from 20 to 60 nm (diameter) by increasing the reaction time (Figure 3A).[29,31] Using dodecanethiol as the sulfur source instead, *via* a heat-up protocol at 245 °C with a ten hour reaction time, led to single-layer nanosheets; as noted above, this was attributed to the slow decomposition of dodecanethiol generating a low concentration of H_2S over the course of the ten-hour reaction time, promoting kinetic control of lateral growth, as opposed to the "burst" of H_2S from the rapid decomposition of CS_2 (Figure 3C).[21] This was further supported by test reactions using H_2S gas directly, which was injected either rapidly (mimicking CS_2 decomposition) or slowly over ten hours (mimicking dodecanethiol decomposition); this replicated the aforementioned observations, with rapid H_2S injection leading to multilayer nanodiscs and slow injection leading to large nanosheets, although the quality of the materials was not as high, possibly due to the inhomogeneity of the gas mixing into the solution phase.

In a more recent report, attempts to prepare ZrS_2 nanocrystals from $ZrCl_4$ and thiourea using either octadecene (ODE) or octadecene and oleic acid (9:4 vol/vol ratio) as the solvent were described; however, the results were ambiguous since only ZrO_2 was observed during EDX and XPS characterization of the resulting materials.[32]

The heat-up reaction of $ZrCl_4$ with elemental Se (2.0 equiv) at 300 °C gave rise to $ZrSe_3$ nanoplatelets approximately 20 nm in diameter, as reported by Cheon *et al*.[29] $ZrSe_3$ is a layered compound that can best be viewed as containing Zr^{4+} with one Se^{2-} ion and one Se_2^{2-} ion per cation; no colloidal syntheses of the diselenide $ZrSe_2$ have been reported.

Binary Hafnium Chalcogenides. Multilayer nanodiscs and single layer nanosheets of HfS_2, as well as nanoplatelets of $HfSe_3$, have been prepared by the Cheon group using protocols

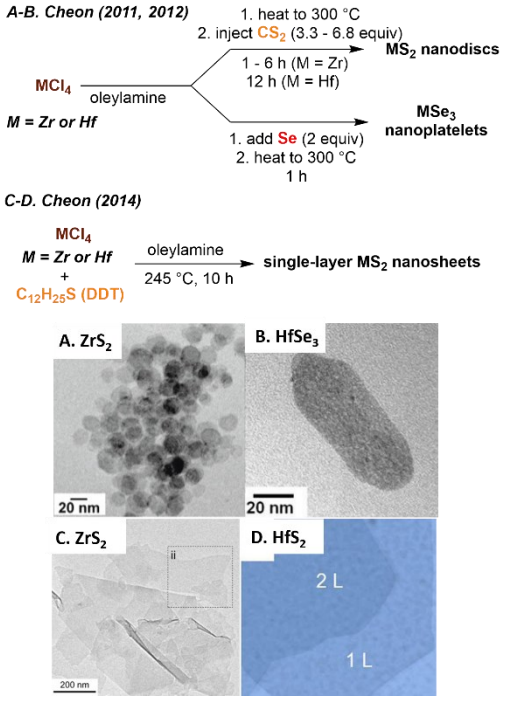

Figure 3. (A-B) Synthetic approaches to HfS_2 and ZrS_2 nanodiscs or $HfSe_3$ and $ZrSe_3$ nanoplatelets, showing TEM images of ZrS_2 (A) and $HfSe_3$ (B) particles as representative examples. ZrS_2 particles shown in (A) were prepared with a reaction time of 1 h and 3.3 equivalents of CS_2. Adapted with permission from J. Jang, S. Jeong, J. Seo, M.-C. Kim, E. Sim, Y. Oh, S. Nam, B. Park, and J. Cheon, *J. Am. Chem. Soc.* 2011, **133**, 7636-7639, copyright 2011 American Chemical Society, and from S. Jeong, D. Yoo, J. Jang, M. Kim, and J. Cheon. *J. Am. Chem. Soc.* 2012, **134**, 18233-18236, copyright 2012 American Chemical Society. (C-D) Preparation of single-layer ZrS_2 and HfS_2 nanosheets, showing TEM image of ZrS_2 nanosheets (scale bar is 200 nm) and pseudocolor TEM image of HfS_2 nanosheets with layer numbers given. Adapted with permission from D. Yoo, M. Kim, S. Jeong, J. Han, and J. Cheon. *J. Am. Chem. Soc.* 2014, **136**, 14670-14673. Copyright 2014 American Chemical Society.

virtually identical to those described above for the zirconium analogues, with $HfCl_4$ as the metal precursor (Figure 3B,D).[21,29] For the synthesis of HfS_2 multilayer nanodiscs *via* hot injection of CS_2, a longer reaction time was used compared to ZrS_2 (12 h instead of 1-6 h). Compared to the well-defined and circular ZrS_2 nanodiscs, the HfS_2 particles were more irregular with poorly-defined edges.

Ternary Group 4 Transition Metal Chalcogenide Nanomaterials

As noted in the introduction, the most prominent group of ternary group 4 transition metal chalcogenides are those with general formula $(AE)M^{4+}Q_3$, including the chalcogenide perovskites $BaZrS_3$ and $BaHfS_3$, as well as the non-perovskite material $BaTiS_3$.

Barium Titanium(IV) Sulfide. Our group has developed three routes to the synthesis of $BaTiS_3$ colloidal nanomaterials, which are illustrated in Figure 4. We initially reported the solution-phase synthesis of colloidal nanorods and nanoparticles of $BaTiS_3$ using metal amide precursors with N,N'-diethylthiourea as the sulfur source (Figure 4A-B).[33] Two different synthetic protocols were employed, which gave rise to nanocrystals with different morphologies: a hot-injection approach and a heat-up approach.

The metal precursors used in this synthesis, $Ti(NMe_2)_4$ and $Ba[N(SiMe_3)_2]_2(THF)_2$, were chosen due to their high solubility in nonpolar solvents such as oleylamine at room temperature, their lack of oxygen content, and their anticipated high reactivity towards the H_2S which is believed to be formally generated *in situ* by decomposition of N,N'-diethylthiourea. These factors differentiate them from the simple metal salt precursors which are frequently used in nanocrystal synthesis, such as acetates and acetylacetonates. Although titanium(IV) halides can be dissolved in oleylamine as noted above, barium halides are insoluble, disfavoring the use of halide-containing precursors. Similarly, oleylamine was selected as the sole solvent and ligand due to its relatively weak coordinating ability and lack of oxygen content. We hypothesized that the metal amide precursors undergo transamidation with oleylamine *in situ*, resulting in the formation of metal oleylamide complexes.[33] Even with these reactive precursors, we found that a minimum temperature of 280 °C was required to form any of the desired product. This limitation does not appear to be due to the reactivity of the thiourea precursor, since similar N,N'-dialkylthiourea precursors are known to give rise to other metal sulfide (e.g. lead sulfide) nanomaterials at temperatures at least as low as 150 °C;[34] rather, this may be related to a minimum temperature required to achieve crystallization of $BaTiS_3$ material from monomers. We also found that a significant excess of the sulfur source was necessary for producing phase-pure materials; generally, 30 equivalents (i.e., a ten-fold excess) of N,N'-diethylthiourea were used.

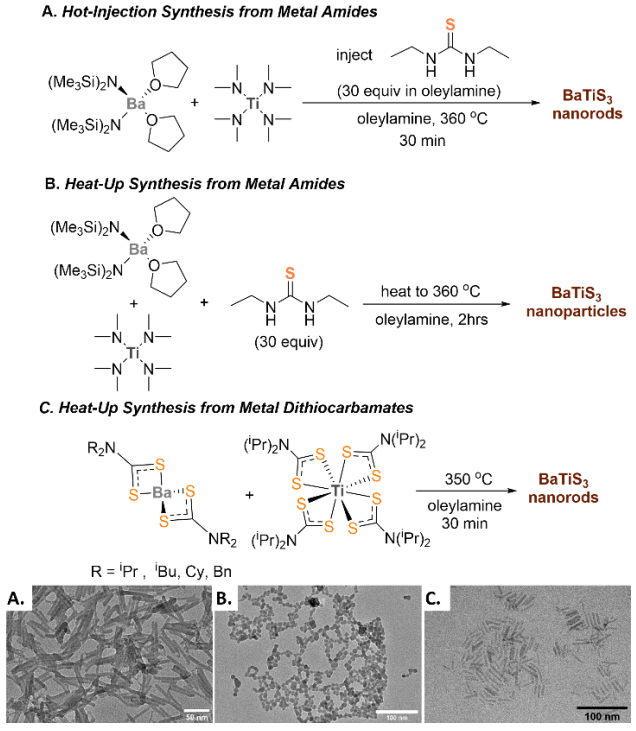

Figure 4. (A-B) Two methods for the preparation of $BaTiS_3$ nanorods and nanoparticles from metal amide precursors. TEM scale bars are 50 nm (A) and 100 nm (B). Adapted with permission from D. Zilevu and S. E. Creutz, *Chem. Mater.* 2012, **33**, 5137-5146. Copyright 2021 American Chemical Society. (C) Synthesis of $BaTiS_3$ nanorods from metal dithiocarbamate precursors; TEM image is shown for particles generated from precursor with R = ^{i}Bu. TEM image is reproduced from reference 37 with permission from The Royal Society of Chemistry.

Using a hot-injection approach under our standard conditions (360 °C and a 27 mM concentration of metal precursors in oleylamine), we produced fairly uniform $BaTiS_3$ nanorods with widths of approximately 6 nm and lengths of approximately 50 nm (Figure 4A). We found that the size and aspect ratio of the particles produced by hot injection could be tuned by changing the reaction concentration; when the concentration was decreased to 10 mM, nearly isotropic particles with an average width of about 10 nm and a 1.4:1 aspect ratio were formed instead of nanorods.

Nanocrystals prepared using a heat-up approach under otherwise similar conditions (360 °C and 27 mM concentration, Figure 4B) instead had a nearly isotropic shape, illustrating that the nanocrystal morphology could be controlled either by synthesis method or by reaction concentration.

Colloidal solutions of the $BaTiS_3$ nanorods showed strong absorbance throughout the visible and near-infrared ranges, featuring a strong peak near 1500 nm whose exact energy varied from sample to sample (Figure 5B).[33] Crystallographic analysis of the nanorods showed reasonable agreement with the known structure of bulk $BaTiS_3$. Slight deviations of the peaks from the calculated positions are related to the unique structural characteristics of this material; it is characterized by an incommensurate composite structure with two interpenetrating sublattices and stoichiometry-dependent lattice parameters (Figure 5A), which are discussed in more detail in our original report.[33,35,36] The evolution of the crystallographic and optical properties as a function of reaction time was studied, and we found that although nanorod growth appeared to be complete within the first five minutes of reaction, the stoichiometry continued to change over time, with the nanorods becoming increasingly sulfur-deficient as the reaction time increased, generally reaching a stoichiometry corresponding to around $BaTiS_{2.85}$ after 30 minutes. The mechanism of charge compensation in the off-stoichiometric compounds is currently unknown but could be related to redox state changes of the titanium ions or the buildup of free carriers; notably, we found that the energy of the ~1500 nm absorbance band also increased concomitantly with the change in stoichiometry. The stoichiometric changes observed with increasing reaction time could have important implications for controlling the optical properties of this and related materials, including the luminescence properties of chalcogenide perovskite nanomaterials (*vide infra*).

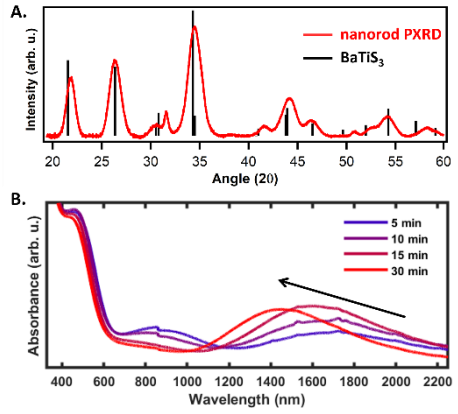

Figure 5. (A) Powder X-ray diffraction data for $BaTiS_3$ nanorods produced using hot-injection method from metal amide precursors. Reference data is for $P6_3/mmc$ phase. Slight shifts between reference and sample data are due to off-stoichiometry of the material. (B) Changes in the optical spectra of $BaTiS_3$ nanorods from hot-injection synthesis with increasing reaction time. Adapted with permission from D. Zilevu and S. E. Creutz, *Chem. Mater.* 2012, **33**, 5137-5146. Copyright 2021 American Chemical Society.

We later reported an alternative pathway to synthesize colloidal $BaTiS_3$ nanocrystals by using metal dithiocarbamate complexes as precursors *via* a heat-up approach in oleylamine at 350 °C (Figure 4C).[37] While the use of metal dithiocarbamate complexes as a "single-source precursors" for the preparation of metal chalcogenide thin films and nanocrystals is fairly well known, our work was the first reported example of the use of a group 4 transition metal dithiocarbamate complex as a colloidal nanocrystal precursor.[38] To prepare $BaTiS_3$, we combined a previously known homoleptic titanium(IV) N,N-diisopropyldithiocarbamate complex with one of four novel barium N,N-dialkyldithiocarbamate complexes that we prepared with different alkyl substituents (isopropyl, isobutyl, benzyl, and cyclohexyl).[39] These precursors have some significant advantages over the barium amide precursor $Ba[N(SiMe_3)_2]_2(THF)_2$ used in our previous route, due to their ease of synthesis and air stability.

The nanocrystals produced by decomposition of the metal dithiocarbamate precursors were qualitatively similar to those produced from the metal amide precursor-based hot injection route described above, generally exhibiting a nanorod-like morphology and strong near-IR absorbance features; however, the morphology was less uniform and somewhat less reproducible.[37] Furthermore, we found that the different substituents on the barium dithiocarbamates had no systematic effect on the outcome of the synthesis in terms of the nanocrystal properties; we believe that this is due to the fact that transamidation of the dithiocarbamates with oleylamine occurs *in situ* prior to decomposition to form the metal sulfides (*vide infra*).

Recently, the Agrawal group reported the preparation of $BaTiS_3$ thin films prepared in part from a solution-phase molecular precursor.[40] Although not colloidal nanomaterials, the chemical principles behind such solution-phase thin film deposition protocols have some commonalities with colloidal nanocrystal preparation; the same route was also used to prepare $BaZrS_3$ thin films and is discussed further below.

Barium Zirconium(IV) Sulfide. Of all the materials discussed in this article, $BaZrS_3$ has been the subject of perhaps the most intense interest and investigation over the last few years because of its status as a chalcogenide perovskite. The general structural and optoelectronic properties of $BaZrS_3$ and other chalcogenide perovskites in bulk and as thin films have been recently reviewed.[1]

The first report of colloidal $BaZrS_3$ nanocrystals involved a "top-down" method: the Nag group prepared bulk powders of $BaZrS_3$ *via* a traditional solid-state synthesis at elevated temperature (600 °C), then finely ground the powders and isolated a sub-population of nanosized particles.[2] Colloidal suspensions were successfully prepared by heating the

nanocrystal powder to 120 °C in N-methyl-2-pyrrolidinone (NMP); further heating to 160 °C in the presence of oleylamine and concomitant removal of NMP produced ligand-modified nanocrystals that could be dispersed in chloroform.

Notably, in this same report, the Nag group also discussed their unsuccessful attempts to carry out a direction solution-phase synthesis of colloidal $BaZrS_3$ nanocrystals, via a protocol involving hot injection of CS_2 into a mixture of $BaCl_2$ and $ZrCl_4$ in oleylamine at 300 °C; only binary phases such as BaS and ZrS_2 were detected in the products by PXRD.[2] We reported that our own early attempts to prepare $BaZrS_3$ nanocrystals using $BaCl_2$, $ZrCl_4$, and CS_2 or S_8 in oleylamine were similarly unsuccessful, giving rise to no crystalline products at 240 °C, although the low temperature tested may have precluded success in this case.[3] The poor solubility of $BaCl_2$ in oleylamine is likely at least in part to blame for these failures.[4] We attempted to solve the solubility issue by using metal acetate and acetylacetonate salts ($Ba(OAc)_2$ and $Zr(acac)_4$) in the presence of oleic acid at 300 °C, but this gave rise only to unidentified nanocrystalline materials, not $BaZrS_3$; we suspect that strong binding of oleate to the oxophilic Zr^{4+} likely significantly attenuates its reactivity, precluding formation of relatively weaker Zr-S bonds, and possibly leading to the formation of oxides through decomposition of the carboxylate groups at elevated temperatures.[3] Nag *et al.* also speculated in their report that more reactive metal precursors may be more likely to give rise to the desired ternary $BaZrS_3$ product.[2]

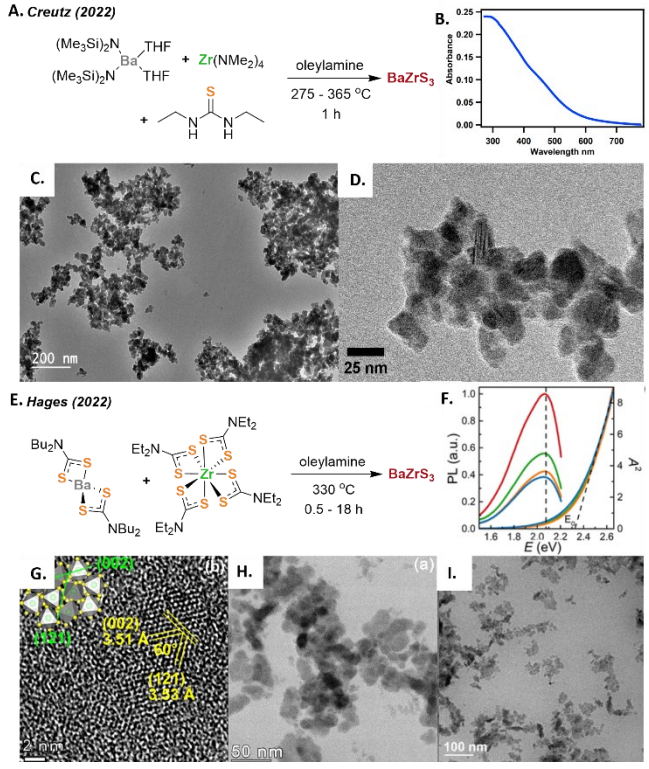

Figure 6. Solution syntheses of $BaZrS_3$ nanocrystals. (A) Heat-up synthesis based on metal amide precursors and UV-Vis absorbance spectrum (B) and TEM images (C-D) of the resulting nanocrystals. Reproduced from reference 3 with permission from The Royal Society of Chemistry. (E) Heat-up synthesis based on metal dithiocarbamate precursors and UV-Vis absorbance and photoluminescence spectra (F) and TEM images (G-I) o f the resulting nanoparticles. Reprinted with permission from R. Yang, A. D. Jess, C. Fai, and C. J. Hages, *J. Am. Chem. Soc.* 2022, **144**, 15928-15931. Copyright 2022 American Chemical Society.

In 2022 two successful procedures for the solution-phase synthesis of colloidal $BaZrS_3$ nanocrystals were independently reported by our group and the Hages group (Figure 6).[3,4] We employed a similar protocol to that we developed for the synthesis of $BaTiS_3$ (*vide supra*), consisting of the combination of metal amide precursors $Zr(NMe_2)_4$ and $Ba[N(SiMe_3)_2]_2(THF)_2$ with N,N'-diethylthiourea as the sulfur source in oleylamine *via* a heat-up procedure to final reaction temperatures between 275 – 365 °C (Figure 6A).[3] The reaction required a large excess of N,N'-diethylthiourea (~60 equivalents) and a high concentration in order to consistently give rise to $BaZrS_3$ without detectable impurities. Analogously to our experience with $BaTiS_3$, we attribute the success of this protocol to the use of highly soluble and reactive metal precursors and the absence of any oxygen-containing ligands or other moieties that could bind strongly to the oxophilic zirconium(IV) cation, reducing its reactivity and/or give rise to oxide impurities.

The nanoparticles resulting from this synthetic route were relatively non-uniform (~20 nm in diameter) and had a platelet-like appearance by TEM (Figure 6C-D); the size and anisotropic particle shape were also confirmed by Rietveld refinement of the PXRD data, suggesting that the individual particles are mostly monocrystalline rather than polycrystalline. Although the particles formed colloidal suspensions, they tended to appear highly aggregated by TEM, suggesting that ligand coverage was inadequate to give rise to well-dispersed independent particles, possibly due to the use of only relatively weakly binding oleylamine ligands in the synthesis.

The nanoparticles we prepared under optimized conditions at 365 °C (designated HT-$BaZrS_3$) showed powder X-ray diffraction in good agreement with the expected pattern based on the known orthorhombic distorted perovskite *Pnma* structure, which was originally indexed by Clearfield in 1963, fully determined by Lelieveld and Ijdo in 1980 using neutron powder diffraction, and later confirmed by Niu *et al.* using single-crystal X-ray diffraction (Figure 7).[41–43] An earlier (1956) report of a purported low-temperature tetragonal modification was indexed by Hahn and Mutschke, but has seemingly not been reproduced since.[44]

However, nanocrystals prepared by our method at lower temperatures (designated LT-$BaZrS_3$, down to 275 °C) showed signs of structural changes.[3] While X-ray pair-distribution-function (PDF) analysis demonstrated that the local structure was still similar to the reported distorted perovskite phase, shifts and new features became apparent in the PXRD (see Figure 7), suggesting changes in the long-range ordering. These features could not be attributed to a known impurity such as a binary sulfide or an oxide; moreover, since the appearance of new peaks consistently occurred concomitantly with small but noticeable shifts in the positions of other features as well as a decrease in the intensity of the prominent peak at 36° 2θ, we suggested that these changes were due to structural changes rather than the presence of an unidentified impurity.

The Hages group reported a solution-phase synthesis of $BaZrS_3$ colloidal nanocrystals based on the decomposition of

metal dithiocarbamate precursors (Figure 6E).[4] Anhydrous homoleptic Ba^{2+} and Zr^{4+} dithiocarbamate complexes, $Ba(S_2CNBu_2)_2$ and $Zr(S_2CNEt_2)_4$, were prepared, combined in oleylamine at high concentration, and heated at a slow controlled rate (5 °C/min) to 330 °C; the reaction was allowed to proceed for times between 30 minutes to 18 hours. The resulting nanoparticles were non-uniform (10-20 nm diameter) and platelet-like in appearance, similar to ours, and individual particles were observed to consist of multiple smaller crystalline domains (< 5 nm size) (Figure 6G-I).

PXRD analysis of the resulting nanoparticles showed prominent diffraction peaks largely in agreement with those expected based on the reference data for the distorted orthorhombic *Pnma* perovskite; however, the occurrence of several additional features at approximately 22°, 30°, and 33° 2θ was noted (Figure 7).[4] It was suggested that these may result from impurities (e.g. oxides) or an unidentified zirconium-rich phase, based on comparison to previously reported data for related thin films.[45] However, comparison to our data (see Figure 7) shows that the diffraction pattern reported by Hages *et al.* is a good match for our low-temperature phase, LT-$BaZrS_3$—specifically, these extra features are also observed in our data, along with the absence of the expected feature at 36° 2θ, the appearance of a clear shoulder at 43° 2θ, and a small but definitive shift to higher angles in the location of the peaks near 44.5° and 52° 2θ. Therefore, we suggest that rather than impurities, the observed features may arise from the modified LT-$BaZrS_3$ phase discussed above, although given that the exact structure of this phase is not yet definitively characterized, other possibilities cannot be strictly ruled out.

Despite the different synthetic routes and some differences in the resulting properties, the $BaZrS_3$ nanoparticles reported by us and by Hages *et al.* showed broadly similar structural and morphological properties, suggesting some generality to the solution-phase synthesis of $BaZrS_3$.[3,4] Interestingly, these two reports also gave rise to a number of similar unanswered questions, indicating clear directions for necessary future research. First, as discussed in the previous paragraphs, the structure of some of the nanomaterials synthesized—especially at temperatures below 365 °C—differs in small but potentially significant ways from the structure determined for bulk powders and single crystals of $BaZrS_3$; while our PDF data

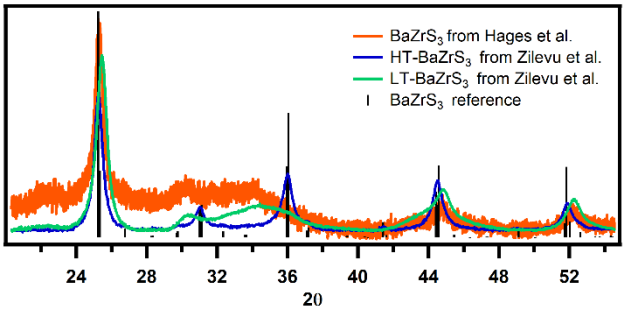

Figure 7. Comparison of the powder X-ray diffraction patterns for $BaZrS_3$ nanoparticles produced by Hages *et al.* (orange, from reference 4) and LT-$BaZrS_3$ and HT-$BaZrS_3$ nanoparticles from reference 3. Data is compared with reference pattern for distorted perovskite (*Pnma*) $BaZrS_3$ from Lelieveld and Ijdo (reference 42). The data from Hages *et al.* was digitized from data presented in reference 4 and a segmented linear baseline correction was applied to facilitate comparison to the other data.

suggests that the local structure remains similar (i.e., perovskite-like), further data and analysis is necessary to reach a complete understanding of its crystallographic phase, and to better control and select for the structural outcomes of the synthesis. Second, the surface properties and stabilization of the nanocrystals remains a major unknown, especially with respect to the colloidal stability of the nanomaterials and their tendency to aggregate, which was observed to varying extents in both reports.

Third, the factors that lead to luminescence—or a lack thereof—from the nanomaterials remain largely unknown. While Hages *et al.* observed luminescence in their materials (Figure 6F), with luminescence intensity and lifetime both increasing as a function of reaction time, we observe no detectable luminescence from our materials (which were prepared with a relatively short reaction time of 30 minutes). This could be related to surface properties or other defects which are not readily observed; curiously, the Hages group isolated two different populations of nanocrystals from the workup of their reactions—a non-dispersible fraction that was not luminescent, and their final colloidally stable fraction of nanoparticles that was luminescent, despite no obvious morphological or structural differences between the two based on TEM and PXRD characterization. It will be interesting to attempt to better elucidate the changes that occur during the course of the extended reaction times and attempt to understand the source of these differences. For instance, in the case of $BaTiS_3$ (*vide supra*), changes in the stoichiometry of the materials were observed with increasing reaction time; if a similar process is operative in $BaZrS_3$ it could account for some of the observed changes.[33]

Both our approach and that of Hages *et al.* also showcase some of the key considerations in the selection of appropriate precursors, solvents, and reaction conditions for the successful synthesis of these ternary early transition metal chalcogenides, which are apparent throughout the examples discussed here, including the need to use reactive metal precursors lacking oxygen-containing ligands and weakly-binding ligands such as oleylamine. These considerations are discussed further later in this review.

In addition to the colloidal nanocrystals of $BaZrS_3$, there has been some success in the solution processing of $BaZrS_3$ thin films from molecular precursors, whose discussion is warranted in this context since similar chemical considerations apply in these two scenarios. The Agrawal group found that thin films of $BaZrS_3$ could be generated by combining a soluble barium dithiolate complex ($Ba(S^tBu)_2$, produced by the reaction of Cp^*_2Ba with HS^tBu) with zirconium hydride (ZrH_2) nanopowder in butylamine to create a slurry which could be drop-cast and annealed under sulfurization conditions to at least 550 °C to produce phase-pure $BaZrS_3$ films; however, these were not true soluble molecular precursors since the ZrH_2 is supplied as a colloid, limiting the film quality (Figure 8A).[40]

This issue was circumvented in a more recent report by Agrawal in collaboration with the Bart group, in this case using true solution-phase molecular precursors for thin film fabrication.[46] In this report, a barium bis(dithiocarboxylate)

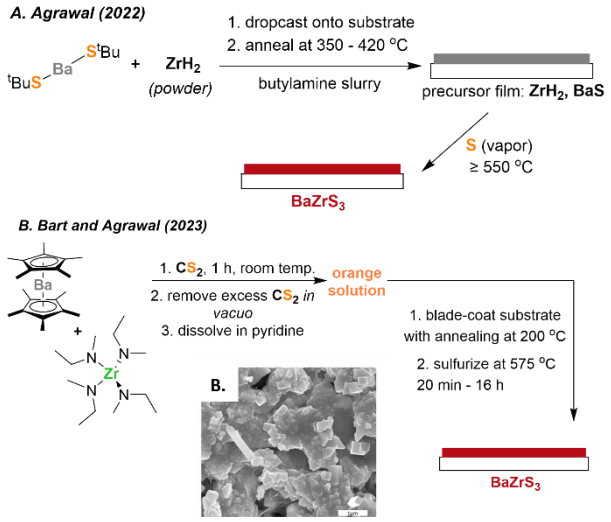

Figure 8. Preparation of $BaZrS_3$ thin films from solution-phase precursors. (A) Combining barium bis(*t*-butylthiolate) and metal hydride nanopowders forms an initial BaS and metal hydride film, which is annealed and sulfurized to form $BaZrS_3$. (B) Barium bis(permethylcyclopentadienyl) and zirconium tetrakis(methylethylamide) precursors react in CS_2 to produce an orange solution containing barium dithiocarboxylate and zirconium dithiocarbamate precursors, as well as possible mixed-ligand species formed *in situ*. Blade coating and annealing/sulfurization produces $BaZrS_3$ film, whose SEM image is shown (scale bar 1 µm). Adapted with permission from reference 46.

complex and a zirconium tetrakis(dithiocarbamate) complex, both of which are generated *in situ* by insertion reactions of CS_2 into the appropriate precursor complex, are combined in pyridine solution, deposited by blade-coating, annealed, and sulfurized at 575 °C to produce $BaZrS_3$ (Figure 8B).

A number of interesting chemical phenomena were observed in this process, including ligand exchange between the barium and zirconium precursors that was speculated to contribute to the successful formation of ternary $BaZrS_3$ without the appearance of binary sulfides upon initial decomposition.[40] In both of these thin film preparations, the authors observed that the luminescence of the films significantly increased after prolonged sulfurization/annealing, starting from essentially no luminescence at short annealing times (< 1 h); it is notable that a similar phenomenon was observed by the Hages group in their nanocrystals.[4] Despite their success, these thin film preparations still suffer from the significant drawback of requiring high-temperature annealing and sulfurization steps after deposition. Nevertheless, the new precursor chemistry developed using barium thiolate, barium dithiocarboxylates, and metal hydrides suggests potential avenues for further development of solution-phase colloidal nanocrystal synthesis as well.

Barium Hafnium Sulfide. No examples of colloidal nanocrystals of barium hafnium sulfide have yet been reported by any synthetic route. However, Agrawal and Bart have reported the preparation of $BaHfS_3$ thin films from solution-phase molecular precursors, by an extension of the protocols described above for the preparation of $BaZrS_3$ thin films.[46]

Binary Group 5 Transition Metal Chalcogenide Nanomaterials

All binary group 5 sulfides and selenides including VS_2, VSe_2, NbS_2, $NbSe_2$, TaS_2, and $TaSe_2$, have been prepared as colloidal nanomaterials, although the heavier congeners are not as well studied.

Binary Vanadium Chalcogenides. Vanadium chalcogenides, including VS_2, VSe_2, and VS_4, are among the most facile to synthesize of the materials discussed in this review, likely due to the relatively low oxophilicity and hardness of vanadium (*vide infra*); as a result, examples of these materials are much more widely known (Figure 9). Even numerous hydrothermal routes using aqueous media have been reported to produce VS_2 and VSe_2, although in many cases the hydrothermal approach yields

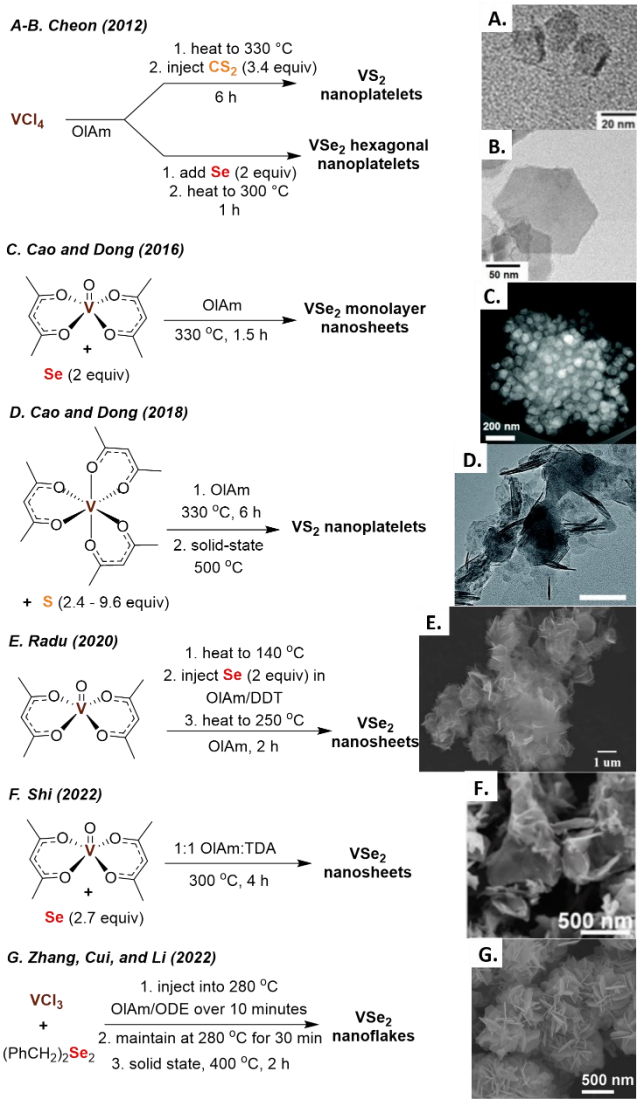

Figure 9. (A-B) Preparation of VS_2 (A) and VSe_2 (B) nanoplatelets using general methodology. Adapted with permission from S. Jeong, D. Yoo, J. Jang, M. Kim, and J. Cheon. *J. Am. Chem. Soc.* 2012, **134**, 18233-18236. Copyright 2012 American Chemical Society. (C) Synthesis and dark-field TEM image of approximately 0.4 nm-thick VSe_2 nanosheets; adapted from reference 57 with permission from the Royal Society of Chemistry. (D) Synthesis of VS_2 nanoplatelets and TEM image of agglomerated particles with 50-60 nm lateral size; TEM image corresponds to particles prepared with 9.6 equivalents of sulfur. Reproduced from reference 58 with permission from the Royal Society of Chemistry. (E) Synthesis of VSe_2 nanosheets and SEM image of agglomerated nanosheets; reproduced from reference 60 and licensed according to https://creativecommons.org/licenses/by/4.0/. (F) Synthesis of VSe_2 nanosheets and SEM image, adapted with permission from reference 59, © 2022 Wiley-VCH GmbH. (G) Synthesis of VSe_2 nanoflakes and SEM image of aggregated flakes, adapted with permission from reference 61, © 2022 Wiley-VCH GmbH.

bulk material which must be further exfoliated to generate nanoparticles or nanostructured materials.[47–50]

The synthesis of VS_4 nanomaterials with nanorod, nanosheet, and nanoflower morphologies has been achieved solvothermally in various mixed aqueous-organic media, including by microwave-assisted routes, using thioacetamide or cysteine as a sulfur precursor and ammonium vanadate or vanadyl acetoacetonate as the vanadium source.[51–53] The effect of solvent, precursors, reaction time, concentration, and order of addition were all studied in detail.[51] Anhydrous N-methyl-2-pyrrolidone (NMP) or dimethylformamide (DMF) were also successfully used as reaction media for nanostructured VS_4 synthesis, but with more agglomeration and poorer morphological control, suggesting that a small amount of water played an important role in producing discrete nanocrystals.[51] Interestingly, it is apparently possible to prepare either VS_2 or VS_4 using the same precursors (vanadyl acetoacetonate and cysteine) and solvent (NMP), depending on the specific reaction conditions used.[51,54] VSe_2 nanosheet assemblies could also be prepared under solvothermal conditions in NMP from vanadyl acetoacetonate, SeO_2, and formic acid, which were proposed to generate H_2Se *in situ;* the formic acid likely also functions as a reducing agent. Alternatively, selenium powder could be used as the anion precursor in DMF solution, in combination with hydrazine hydrate as a reductant.[55,56] However, it should be emphasized that due to the lack of stabilizing ligands, the examples described in this paragraph are nanostructured, but not necessarily colloidal.

In purely organic surfactant solutions, the syntheses of colloidal nanocrystalline VS_2 and VSe_2 were first reported by the Cheon group using their general route to transition metal dichalcogenide nanoplatelets with VCl_4 as the metal precursor and CS_2 as the sulfur source in oleylamine (Figure 9A-B).[29] However, most subsequent reports have used less reactive and easier-to-handle precursors, especially vanadium(III) acetylacetonate, $V(acac)_3$, and vanadyl acetylacetonate, $VO(acac)_2$. Cao and Dong have reported the synthesis of colloidal VS_2 and VSe_2 under similar conditions (Figure 9C-D).[57,58] Monolayer nanosheets of VSe_2 were produced from the combination of elemental selenium powder and $VO(acac)_2$ in oleylamine solution at 330 °C for 1.5 hours; other solvents or lower reaction temperatures were found to give rise to impurities including vanadium oxides (Figure 9C).[57] On the other hand, thin colloidal VS_2 nanoplatelets were produced from $V(acac)_3$ and varying amounts of elemental sulfur powder in oleylamine at 330 °C for 6 hours; however, the materials were also further subjected to solid-state annealing at 500 °C (Figure 9D).[58] In both of the above cases, the choice of vanadium precursor was suggested to be critical to the success of the reaction, although specific information about the reaction outcome when a different precursor was used was not provided. Minor modifications of these procedures have been used to optimize the morphologies; for example, the Shi group reported that including tetradecylamine (TDA) in combination with oleylamine (1:1 ratio) in the synthesis of VSe_2 from $VO(acac)_2$ and Se promoted the formation of phase-pure nanosheets that were thinner than counterparts produced without TDA under the same conditions (Figure 9F).[59] Additionally, the Radu group incorporated dodecanethiol as an additional solvent and used a lower reaction temperature (250 °C) to produce highly crystalline VSe_2 nanosheets which were used as precursors for ternary materials (*vide infra*; Figure 9E).[60]

Using a different approach, Zhang, Cui, and Li recently reported the preparation of VSe_2 nanoflakes starting from VCl_3 and dibenzyl diselenide, $(PhCH_2)_2Se_2$, which were co-dissolved in oleylamine and slowly injected into a solution of hot oleylamine at 280 °C (Figure 9G).[61] However, the characterization of the materials was reported only following a solid-state annealing process at 400 °C, so the properties and crystallinity of the as-synthesized materials are unclear.[61] While diorganyl diselenides have been increasingly recognized as useful and tunable precursors for the preparation of colloidal selenide nanocrystals, this report is one of only a couple examples to date of their use in the solution synthesis of early transition metal (groups 3-5) selenides (see below for a second example).[62]

Binary Niobium Chalcogenides. Reports of niobium chalcogenide nanomaterials prepared *via* solution synthesis date back to the 2005 report from the Odom group of the preparation of $NbSe_2$ nanoplatelets and nanowires, although the synthesis required a final high-temperature solid-state annealing step (Figure 10A).[63] In this report, the combination of $NbCl_5$ and elemental selenium in oleylamine or dodecylamine at 280 °C or 250 °C, respectively, for four hours produced a nanostructured precursor phase containing Nb_2Se_9 and Se. Further heating of the solid precursor at 450 °C for three hours led to the formation of $NbSe_2$ nanocrystals whose morphology was dependent on the quenching method used to produce the precursor material—slow cooling at 5 °C/min led to nanoplatelets, while rapid quenching to room temperature by addition of hexane led to nanowires. The morphological change was suggested to be related to the amount of residual solvent (e.g., oleylamine) present in the precursor material used for the subsequent annealing step. This general result was later confirmed by Shi and Ma, who used the same synthesis and annealing conditions to produce either nanorods or nanosheets of $NbSe_2$, depending on whether the reaction mixture was cooled at 20 °C/min or 5 °C/min, respectively.[64] Synthesis of $NbSe_2$ nanoplatelets was also reported by Cheon *et al.* using their general protocol, heating $NbCl_5$ and two equivalents of Se in oleylamine at 300 °C for two hours (Figure 10B). The reason for the difference in the initial product in these cases—an Nb_2Se_9/Se intermediate in the Odom report versus direct formation of $NbSe_2$ in the Cheon report—is not entirely clear, although Cheon *et al.* used a slightly higher temperature and a significantly higher reaction concentration, which may have been sufficient to cause this change.[29] The Radu group has also prepared $NbSe_2$ nanosheets using a hot injection procedure, wherein $NbCl_5$ in oleylamine was injected into a solution of selenium in oleylamine and octadecene at 300 °C. The resulting nanosheets were used as precursors for the preparation of ternary materials (*vide infra*; Figure 10G).[65]

Some recent reports have attempted to shed light more systematically on the factors leading to the preparation of

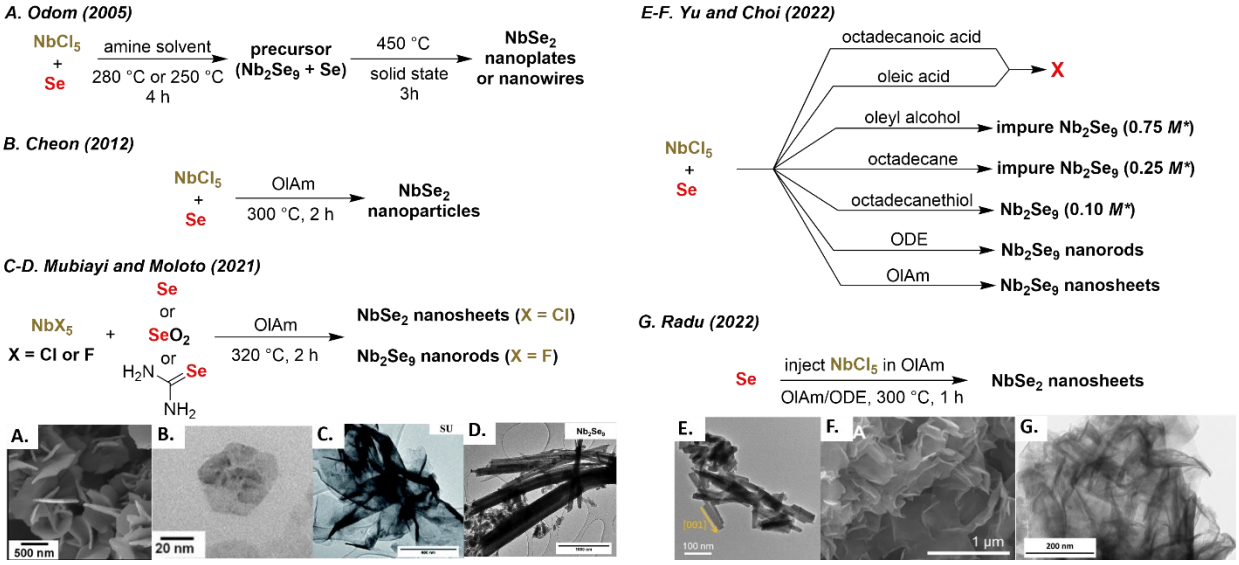

Figure 10. Solution-phase syntheses of niobium selenide materials. (A) Synthesis of nanostructured $NbSe_2$ sample; SEM image shows nanoplates produced in oleylamine at 280 °C, after the solid state annealing step. Adapted with permission from P. Sekar, E. C. Greyson, J. E. Barton, and T. W. Odom. *J. Am. Chem. Soc.* 2005, **127**, 2054-2055. Copyright 2005 American Chemical Society. (B) Preparation of $NbSe_2$ using general procedure for transition metal selenides, and TEM image of a resulting particle. Adapted with permission from S. Jeong, D. Yoo, J. Jang, M. Kim, and J. Cheon. *J. Am. Chem. Soc.* 2012, **134**, 18233-18236. Copyright 2012 American Chemical Society. (C-D) Preparation of $NbSe_2$ nanosheets and Nb_2Se_9 nanorods from different precursors. TEM images show $NbSe_2$ produced from $NbCl_5$ and selenourea (C, scale bar is 400 nm) and Nb_2Se_9 produced from NbF_5 and elemental Se (D, scale bar is 1000 nm). Adapted from reference 66 with permission from The Royal Society of Chemistry. (E-F) Solvent-dependent synthesis of Nb_2Se_9 nanomaterials. (*) Where concentrations are given, these represent the lowest precursor concentration needed to form any Nb_2Se_9, although the product was not necessarily pure under those conditions. In octadecene and oleylamine at least some Nb_2Se_9 formed at all tested concentrations (giving nanorods (E) and nanosheets (F), respectively). Adapted from reference 67 with permission from The Royal Society of Chemistry. (G) Hot-injection synthesis of $NbSe_2$ nanosheets and TEM image (scale bar is 200 nm), reproduced from reference 65 with permission from the American Chemical Society.

different stoichiometries and morphologies of $NbSe_2$ and Nb_2Se_9. The solution synthesis of niobium selenide nanomaterials was recently probed in depth by Mubiayi and Moloto, who described systematically the effect of changing the niobium and selenium precursors (Figure 10C-D).[66] All reactions were carried out in oleylamine using a heat-up methodology at 320 °C for two hours, using four equivalents of the selenium precursor relative to niobium. In all cases, the use of $NbCl_5$ as precursor produced $NbSe_2$ nanosheets while the use of NbF_5 led to a mixture of Nb_2Se_9 nanorods and smaller nanoparticles. With $NbCl_5$, the use of elemental Se, SeO_2, or selenourea could all produce $NbSe_2$, although the materials produced from Se and SeO_2 included significant impurities of niobium(V) oxide. While this oxide impurity could derive from the precursor in the case of SeO_2, in the case of Se it must have resulted from an impurity in the reaction mixture, likely trace water. On the other hand, all three selenium precursors gave rise to Nb_2Se_9 without obvious crystalline impurities when combined with NbF_5.[66] Yu and Choi have recently systematically studied the effect of the organic solvent on the synthesis of Nb_2Se_9 nanorods (Figure 10E-F).[67] They found that, due to the necessity of reducing the precursors *en route* to the target material, the reducing ability of the solvent played an important role in the success of the synthesis, with the more reducing solvents octadecene and oleylamine (or combinations of the two) being most successful; the carboxylic acid solvents oleic acid and octadecanoic acid were completely unsuccessful. Octadecanethiol, oleylalcohol, and octadecane formed Nb_2Se_9 only at relatively higher precursor concentrations. Unfortunately, even under conditions where no oxygen-containing solvents were used, niobium(V) oxide was commonly observed as an impurity, suggesting the presence of adventitious water from non-dried precursors or unintended air exposure during synthesis.

Interestingly, these studies represent some of the only such systematic reports studying the effects of a wide range of precursor or solvent variation within the general class of early transition metal chalcogenides.

Niobium sulfide (NbS_2) colloidal nanomaterials were first reported as part of the general procedure described by the Cheon group, who produced irregularly shaped NbS_2 nanoplatelets using their hot-injection protocol, by heating $NbCl_5$ to 300 °C in oleylamine and injecting 6.8 equivalents of CS_2, followed by a 3 hour reaction time (Figure 11A).[29] A nearly identical protocol was used by Zhu and Yan to produce NbS_2 nanosheets doped with Se, Fe, Co, or Ni, except that a much larger excess of CS_2 (60 equivalents) was supplied, and the product was subjected to solid-state annealing at 400 °C prior to analysis (Figure 11B).[68] Under similar conditions, Mansouri and Semagina found that the synthesis tolerated the inclusion of oleic acid, and a remarkable degree of morphological tunability could be achieved by varying both this solvent ratio and the equivalents of CS_2 used (Figure 11C-F).[69] At a 0.3 oleic acid:oleylamine ratio with 35 equivalents of CS_2, thin multilayer nanoplatelets with well-defined hexagonal facets were formed; increasing the equivalents of CS_2 to 70 or 140 resulted in growth along the *c* axis, increasing the number of layers and ultimately leading to the formation of hexagonal nanorods, with a concomitant decrease in the lateral size relative to the nanoplatelets.[69] In a separate recent report, Xiao and Zhang

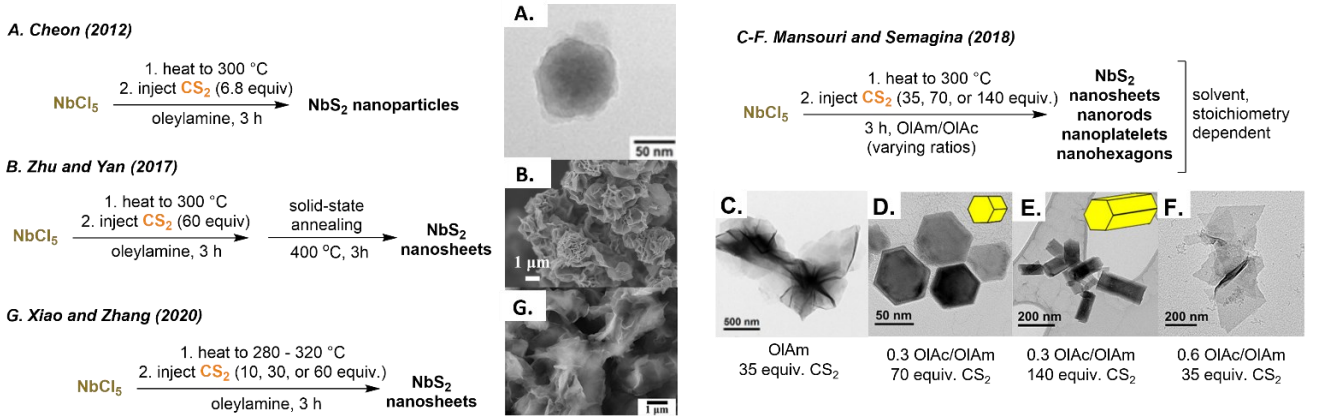

Figure 11. Synthesis of NbS_2 nanomaterials. (A) NbS_2 nanoparticles produced using general synthesis, and TEM image of a resulting particle. Adapted with permission from S. Jeong, D. Yoo, J. Jang, M. Kim, and J. Cheon. *J. Am. Chem. Soc.* 2012, **134**, 18233-18236. Copyright 2012 American Chemical Society. (B) Preparation of nanosheets of NbS_2 and SEM image of flower-like aggregates. Adapted from J. Zhang, C. Du, Z. Dai, W. Chen, Y. Zheng, B. Li, Y. Zong, X. Wang, J. Zhu, and Q. Yan. *ACS Nano* 2017, **11**, 10599-10607. Copyright 2017 American Chemical Society. (C-F) Synthesis of different morphologies of NbS_2 using different solvent mixtures and stoichiometries, with accompanying TEM images. Adapted with permission from A. Mansouri and N. Semagina, *ACS Appl. Nano Mater.*, 2018, **1**, 4408-4412. Copyright 2018 American Chemical Society. (G) Synthesis of NbS_2 nanosheets, with SEM image showing aggregated nanosheets resulting from synthesis at 300 °C with 10 equivalents of CS_2; scale bar is 1 μm. Adapted from reference 70 with permission from Frontiers Media.

replicated the finding that the use of a greater excess of CS_2 tended to result in increased thickness and smaller lateral size, while increasing the reaction temperature (between 280 °C to 320 °C) increased the size in all dimensions (Figure 11G).[70] However, the sole solvent in this case was oleylamine, and all samples were nanosheet-like, confirming that the presence of oleic acid was necessary for the formation of other morphologies. The Radu group has also recently prepared NbS_2 nanosheets *via* slow hot injection of CS_2 into $NbCl_5$ in a mixture of solvents; the resulting particles were used as precursors for ternary material synthesis (*vide infra*) and their detailed characterization was not included in the report.[65]

Binary Tantalum Chalcogenides. There are few reports of solution-synthesized nanomaterials of binary TaS_2 or $TaSe_2$.[29] Odom *et al.* prepared TaS_2 and $TaSe_2$ by routes similar to those they used for $NbSe_2$ (*vide supra*), initially from a dodecylamine solution at 250 °C, but found that the materials were not crystalline until after annealing at >550 °C.[71] The Cheon group included these materials in their report of a general method for transition metal dichalcogenide nanoplatelet synthesis, using methods analogous to those discussed above for other metals (Figure 12A-B).[29] Qiao, Ding, and Sui recently reported using very similar conditions to produce TaS_2 nanosheets (Figure 12E).[72] They found that the morphology of the sample could be altered based on changes to how residual moisture was removed from the system upon initial heating, suggesting an influence of either residual water or small amounts of oxide impurities on the formation and self-assembly of the nanoparticles; under some conditions, a mixture of TaS_2 phases (1T and 2H) was formed. This result again emphasizes the fact that minor changes to the synthesis conditions can influence the outcome in often unpredictable ways.

TaS_2 nanoflakes have also been produced by the Radu group using a mixture of solvents *via* a slow hot-injection approach; a solution of CS_2 in dodecanethiol and oleylamine was prepared and injected dropwise into a solution of $TaCl_5$ in oleylamine and octadecene at 300 °C, followed by a 2 hour reaction time. Large nanoflakes approximately 150 nm in diameter were formed and were used as precursors for the formation of ternary materials (*vide infra*; Figure 12C).[73] $TaSe_2$ nanosheets were also prepared using a heat-up approach (Figure 12D).[73]

Ternary Group 5 Chalcogenides: Sulvanites

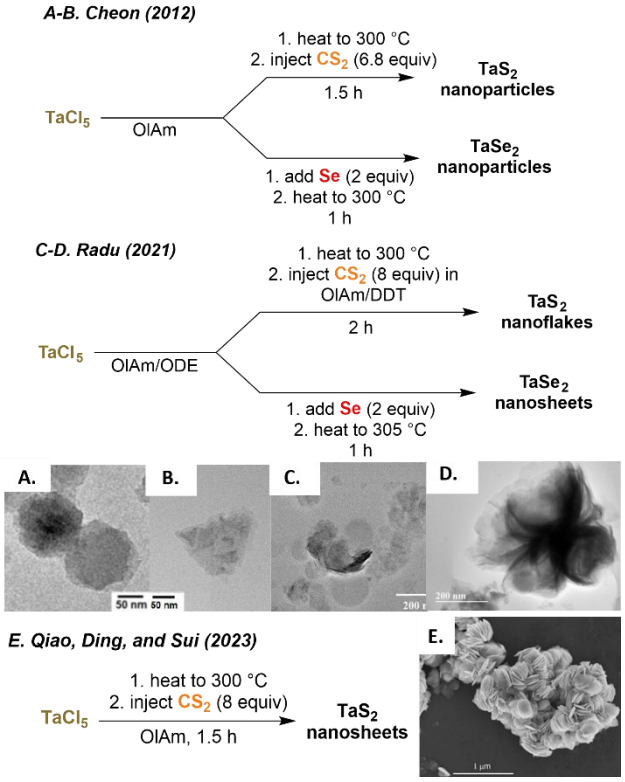

Figure 12. Synthesis of tantalum chalcogenide nanomaterials. (A-B) Synthesis of TaS_2 (A) and $TaSe_2$ (B) nanoparticles using a generalized procedure, with accompanying TEM images. Adapted with permission from S. Jeong, D. Yoo, J. Jang, M. Kim, and J. Cheon. *J. Am. Chem. Soc.* 2012, **134**, 18233-18236. Copyright 2012 American Chemical Society. (C-D) Alternative procedures to access TaS_2 nanoflakes (C) and $TaSe_2$ nanosheets (D) with accompanying TEM images; scale bars are 200 nm. Adapted from reference 73 with permission from MDPI. (E) Synthesis of "accordion-like" aggregates of nanosheets of TaS_2 with SEM image (scale bar is 1 μm). Reprinted from reference 72 with permission from Elsevier.

The only class of ternary group 5 metal chalcogenides that has been significantly explored as colloidal nanomaterials *via* solution-phase synthesis is the sulvanites, with general formula Cu_3MS_4 or Cu_3MSe_4 (M = V, Nb, Ta). These materials have some potential photovoltaic and optoelectronic applications, due to the high absorption coefficients and appropriate bandgaps exhibited by some of the materials (especially Cu_3VS_4). The synthesis and properties of nanoscale sulvanites have recently been reviewed.[6]

Similar to the binary vanadium chalcogenides, the vanadium sulvanites Cu_3VS_4 and Cu_3VSe_4 have been produced by a wide variety of methods, and tolerate the use of oxygen-containing precursors such as vanadyl acetylacetonate ($VO(acac)_2$) and vanadium(III) acetylacetonate ($V(acac)_3$). For example, the Radu group reported the first solution synthesis of nanocrystals of Cu_3VS_4 through the slow hot injection of a sulfur/oleylamine solution into an oleylamine solution of $V(acac)_3$ and $Cu(acac)_2$ (2.4:1 Cu:V ratio) at 230 °C (Figure 13A).[74] A 30 minute reaction time led to approximately 10 nm diameter quasipherical colloidal particles, although an annealing procedure at 600 °C under a sulfur atmosphere was used to improve the crystallinity of the particles.

Shortly thereafter, Buonsanti *et al.* reported a hot-injection protocol wherein a mixture of dodecanethiol and oleylamine was rapidly injected into a mixture of CuI, $VO(acac)_2$, and trioctylphosphine (1:1.33:1 ratio) in octadecene at temperatures ranging from 250 °C to 280 °C, resulting in the formation of high-quality colloidal nanocubes of Cu_3VS_4 whose size could be tuned from 9 to 18 nm based on the reaction temperature (Figure 13B).[75] It was noted that the nanocubes formed stable colloidal solutions as long as anhydrous conditions were maintained, but the use of non-dried solvents resulted in relatively rapid precipitation of the nanocrystals. Interestingly, the authors were able to determine that the mechanism of the reaction most likely involved initial formation of copper sulfide (Cu_2S and CuS) "seeds" that underwent further reaction with vanadium-containing intermediates to produce the final materials. The Radu group later used a similar hot injection procedure to produce Cu_3VSe_4 nanocrystals of somewhat poorly defined cubic shape, based on $VO(acac)_2$, CuCl, and elemental selenium in a combination of oleylamine, trioctylphosphine oxide (TOPO), and oleic acid solvents.[76]

Cu_3NbSe_4, Cu_3TaSe_4, and Cu_3TaS_4 have all been prepared by direct hot injection routes. Wang and Feng prepared Cu_3NbSe_4 by injecting a solution prepared from diphenyl diselenide (Ph_2Se_2) in oleylamine into a hot oleylamine solution of CuCl and $NbCl_5$, producing nanocubes whose size could be tuned through time and temperature variation; using optimized conditions of 280 °C with a 30 minute reaction time produced highly uniform cubes approximately 12 nm in edge length (Figure 13C). It was found that the desired phase was still formed when oleic acid was incorporated as up to about 15% of the solvent, but the nanoparticles became irregularly shaped and non-uniform.[77] Cu_3TaS_4 nanocubes were produced by the Radu group using dropwise hot injection of a CS_2/dodecanethiol/oleylamine mixture into a solution of $TaCl_5$ and $CuCl_2$ in oleylamine and octadecene; they used the inverse order of injection to prepare Cu_3TaSe_4 nanoparticles by rapidly injecting a $TaCl_5$/$CuCl_2$/oleylamine/octadecene precursor mixture into a solution of elemental selenium in oleylamine/octadecene that had been heated to 300 °C.[73] The Cu_3TaSe_4 particles had a poorly defined core-shell-like morphology. Mechanistic investigations suggested that both syntheses proceeded *via* initial formation of copper chalcogenide seed phases, similar to the Cu_3VS_4 materials discussed above. This observation was further confirmed by Sanyal and Santra who studied the formation of Cu_3TaS_4 from the hot-injection of CS_2 into CuCl and $TaCl_5$ in oleylamine at 300 °C; they also provided evidence that the transformation of $Cu_{2-x}S$ precursor particles into Cu_3TaS_4 proceeds *via* a vacancy-mediated diffusion process (Figure 13D).[78]

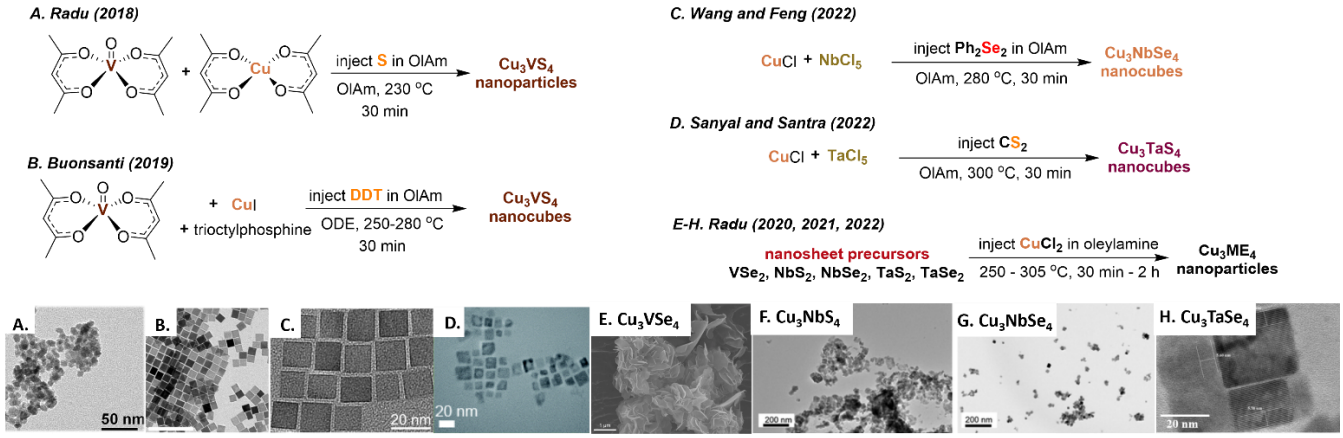

Figure 13. Selected syntheses of sulvanite nanoparticles. (A) Direct synthesis of Cu_3VS_4 nanoparticles, with TEM images adapted from reference 74 with permission from Elsevier. (B) Synthesis of Cu_3VS_4 nanocubes and TEM image of particles synthesized at 280 °C (scale bar is 100 nm). Adapted with permission from V. Mantella, S. Ninova, S. Saris, A. Louidice, U. Aschauer, and R. Buonsanti. *Chem. Mater.* 2019, **31**, 532-540. Copyright 2019 American Chemical Society. (C) Direct synthesis of Cu_3NbSe_4 nanocubes and TEM image of resulting particles. Adapted from reference 77 with permission from The Royal Society of Chemistry. (D) Direct synthesis of Cu_3TaS_4 nanocubes and TEM image of the resulting particles, which were produced using a 1:1 Cu:Ta precursor ratio. Adapted from reference 78 with permission from The Royal Society of Chemistry. (E-H) Cascade synthesis of sulvanite nanoparticles based on addition of Cu^{2+} to MS_2 or MSe_2 precursors (M = V, Nb, Ta). (E) SEM image of Cu_3VSe_4 nanosheets (scale bar is 1 µm) reproduced from reference 60 and licensed according to https://creativecommons.org/licenses/by/4.0/. (F-G) TEM images of nanoparticles of Cu_3NbS_4 and Cu_3NbSe_4, respectively; scale bars are 200 nm, reproduced from reference 65 with permission from the American Chemical Society. (H) TEM image of nanocubes of Cu_3TaSe_4, reproduced from reference 73 with permission from MDPI.

While the evidence suggests that the preparation of sulvanite nanoparticles *via* a direct route involves initial formation of copper chalcogenide precursors, the opposite order of formation has also been deliberately exploited by the Radu group in a "cascade" synthesis, where they prepared VSe_2, NbE_2, and TaE_2 (E = S, Se) nanosheets using methods discussed above, then injected $CuCl_2$ in oleylamine at elevated temperature, resulting in a transformation to sulvanite nanoparticles of varying morphologies (Figure 13E-H). This transformation could be carried out *in situ* without isolating the precursor nanosheets.[60,65,73]

Applications of Early Transition Metal Chalcogenides

Early transition metal chalcogenide nanomaterials exhibit a wide variety of properties, bolstered in part by electronic structures that vary from insulators or wide-gap semiconductors (such as $NaYS_2$), to mid-gap semiconductors (such as $BaZrS_3$), to semi-metals and metallic materials (such as NbS_2); this leads to a broad range of potential applications. In this section, the reported applications of solution-synthesized group 3-5 transition metal chalcogenide nanomaterials are briefly summarized, along with some possible emerging and future applications.

Ion storage, batteries, and supercapacitors. With the exception of Nb_2Se_9, the binary chalcogenides of groups 4 and 5 discussed herein generally exhibit a two-dimensional layered crystal structure, which lends itself well to ion intercalation. As a result, they have been extensively investigated as ion-storage electrodes (Li^+, Na^+, K^+), e.g. for possible applications in rechargeable batteries; importantly, the nanoscale dimensions of solution-synthesized colloidal nanomaterials can be advantageous for these applications, likely due to their higher surface area. For example, when Cheon *et al.* tested the performance of ultrathin ZrS_2 nanodiscs as lithium-intercalation anodes, they showed size-dependent discharge capacity which, for the smallest nanodiscs (20 nm diameter), was 230% enhanced relative to bulk material; the nanoscale materials also exhibited improved stability (Figure 14A).[31] Cao *et al.* compared the performance of solvothermally synthesized VSe_2 nanosheets and bulk material as potential anodes for lithium ion batteries, and similarly found that the nanosheets showed a maximum reversible capacity nearly twice as high (1020 vs. 568 $mAhg^{-1}$) and higher cycling stability as compared to the bulk VSe_2.[56] VS_2, VSe_2, and VS_4 nanomaterials have all also shown promising performance in sodium ion storage, and VS_2 exhibited a high capacity for potassium ion storage, although the specific capacities for the larger ions were smaller than for lithium.[52,54,55] Solution-prepared niobium chalcogenides are also competent for sodium and lithium ion storage, as has been demonstrated for doped NbS_2 nanosheets and Nb_2Se_9 flower-like microclusters; the hierarchical structure of the latter was credited for its improved performance (in terms of specific capacity and stability) relative to rod-like microcrystals of the same material prepared by solid-state synthesis.[68,79] VS_2 nanoplates and NbS_2 nanosheets have also been successfully tested in supercapacitors, where the performance was found to be dependent on the defect density and morphology, respectively.[58,70]

Catalytic applications. Catalysis—including electro- and photocatalysis—is another area where the performance of a number of solution-synthesized early transition metal chalcogenide nanomaterials has been tested. The high surface area of colloidally-prepared nanomaterials has the potential to lead to improved performance relative to bulk materials. Solution-synthesized VSe_2 and TaS_2 nanomaterials have been investigated as electrocatalysts for the hydrogen evolution reaction (HER).[49,57,59,61,72] For example, Cao *et al.* demonstrated that single-layer VSe_2 nanosheets prepared in oleylamine exhibited significantly improved electrocatalytic performance (lower overpotential for a given current density and lower Tafel slope) relative to multilayer nanosheets; they further demonstrated that removal of the native long-chain ligands (which they accomplished by oxygen plasma exposure, OPE) was critical to catalytic performance (Figure 14B).[57] Studies on TaS_2 nanosheets similarly demonstrated superior performance for ultrathin nanosheets over other more highly stacked/aggregated morphologies.[72] Doping and defect engineering have also been used to improve HER catalysis by

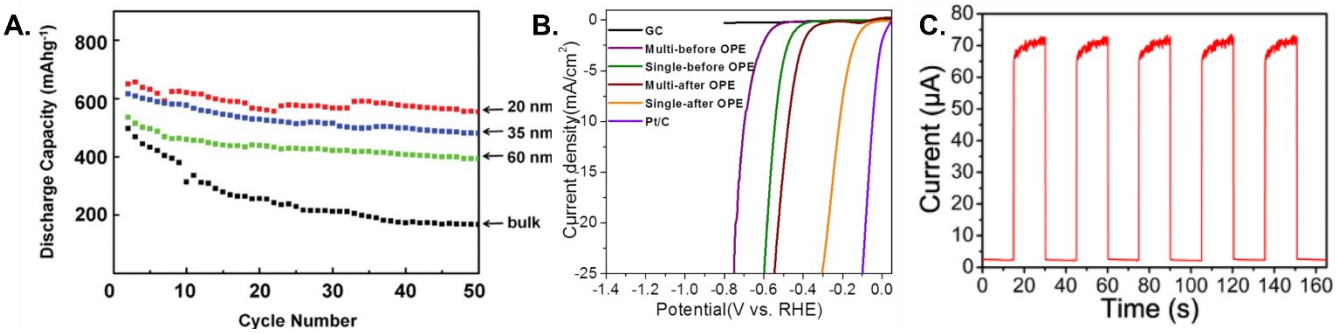

Figure 14. Example applications of solution-synthesized early transition metal chalcogenide nanomaterials. (A) Discharge capacity curves for ultrathin ZrS_2 nanodiscs used in Li^+ intercalation studies. The performance of different nanodiscs with different lateral sizes (red – 20 nm; blue – 35 nm; green – 60 nm) is compared to bulk material. Adapted with permission from J. Jang, S. Jeong, J. Seo, M.-C. Kim, E. Sim, Y. Oh, S. Nam, B. Park, and J. Cheon, *J. Am. Chem. Soc.* 2011, **133**, 7636-7639, copyright 2011 American Chemical Society. (B) Polarization curves for the catalysis of the hydrogen evolution reaction by VSe_2 nanocrystals, comparing single-layer and multi-layer nanosheets before and after oxygen plasma exposure (OPE). Platinium on carbon and glassy carbon (GC) electrodes are also shown for comparison. Reproduced from reference 57 with permission from The Royal Society of Chemistry. (C) Photoresponse of Cu_3NbSe_4 nanocrystal photodector device under white light on/off switching. Reproduced from reference 77 with permission from The Royal Society of Chemistry.

VSe_2 nanoparticles.[49,61] Solution-synthesized VSe_2 nanosheets have also shown excellent activity in electrocatalytic sulfide oxidation, outperforming previously reported materials.[59] Nb_2Se_9 nanocrystals have been demonstrated as electrocatalysts for the oxygen reduction reaction, with morphology-dependent onset potentials and Tafel slopes; nanowires showed considerably superior performance relative to nanosheets, which was attributed to the different catalytic competence of different nanocrystal facets and edges.[67] $NbSe_2$ and Nb_2Se_9 nanocrystals have also been applied as counterelectrodes in dye-sensitized solar cells, where they act to catalyse the reduction of I_3^- to I^-; once again, morphologies with higher surface area tended to show superior performance.[64,66]

Examples of photocatalysis and thermal catalysis are more limited. Cu_3NbS_4 and Cu_3NbSe_4 have been tested for photocatalytic methylene blue degradation using simulated sunlight, with the sulfide material showing a 2.3-times faster rate than the selenide.[65] Mansouri and Semagina deposited NbS_2 nanocrystals with a range of morphologies on an alumina support and tested them as catalysts for the hydrodesulfurization of dibenzothiophene at 325 °C. Nanohexagons—which had the highest proportion of corner and edge sites—showed the fastest rate, which was also about 10 times higher than that observed for bulk NbS_2 under analogous conditions.[69]

Optoelectronic applications. Early transition metal chalcogenide materials that are semiconductors—especially many of the ternary materials, including sulvanites and chalcogenide perovskites—have potential applications in optoelectronic devices including solar cells and photodetectors. In general, the solution-processability of colloidal nanocrystals can make them useful precursors for active layers in thin film devices, motivating the development of routes for their preparation. Most of these colloidal early transition metal chalcogenide semiconductor nanomaterials have only recently been successfully synthesized, and examples of their applications in this area are limited, but some preliminary investigations have shown potentially promising properties.

Excitonic luminescence has been observed from Cu_3VS_4 nanocrystals when shelled with CdS; this example also represents one of the few examples of a core/shell heterostructure developed using a solution-synthesized early transition metal chalcogenide nanomaterial.[80,81] Cu_3VSe_4 nanocrystals also show luminescence, and have exhibited a photocurrent response in photoelectrochemical cells, with nanosheets giving a 9-fold higher current response than roughly cubic-shaped nanocrystals.[60,76] Cu_3TaS_4 and Cu_3TaSe_4 nanocrystals are also luminescent, and Cu_3TaS_4 particles could be successfully processed into conductive films following ligand exchange with S^{2-}.[73] Cu_3NbSe_4 nanocrystals with a band gap of 2.2 eV were successfully processed into photodetector devices with good stability and responsivity under white light irradiation (on/off ratio ~35, Figure 14C).[77]

Solution-synthesized chalcogenide perovskite nanocrystals (e.g. $BaZrS_3$) have not yet been reported in devices, although in some cases they do exhibit luminescence, as noted above.[4] However, $BaZrS_3$ nanocrystals produced by grinding of bulk material have been processed into thin-film field-effect transistors with reasonable electron and hole mobilities (0.017 $cm^2V^{-1}s^{-1}$ and 0.059 $cm^2V^{-1}s^{-1}$, respectively).[2]

Other and emerging applications. A number of other properties and potential applications of early transition metal chalcogenide nanomaterials are predicted based on computations and/or the properties of bulk materials, but have as of yet received little study, or have not yet been successfully realized. For example, as bulk crystals, some of the early transition metal dichalcogenides are low-temperature superconductors, including $NbSe_2$ and TaS_2.[82–84] Although colloidal nanocrystals may be unlikely to exhibit significant practical value as superconducting materials, their study could contribute to an understanding of size-dependent aspects of superconductivity and related correlated-electron behavior.[63] Additionally, as described earlier, the chalcogenide perovskites (e.g. $BaZrS_3$) have been predicted to have considerable potential for applications in photovoltaic and optoelectronic devices, for which solution-processable colloidal nanomaterials could be ideally suited, but this has not yet been successfully realized in the literature.[1,3,4]

Reaction Pathways, General Trends, and Areas for Future Development

The challenges of successfully preparing early transition metal chalcogenide colloidal nanomaterials, especially for groups 3 and 4, are commonly attributed to the fact that these ions, in their typical oxidation states, are hard Lewis acids and highly oxophilic.[85,86] These concepts are quantitatively summarized in Figure 15. In this chart, the height of each element represents its Pearson hardness in the most relevant oxidation state, defined as $\eta = (IE^n - EA^n)/2$, where IE is the ionization energy of the ion with a charge of *n*, and EA is its electron affinity.[87] The elements are further color-coded based on their oxophilicity according to a quantitative scale recently proposed by Kepp.[85] Here, the oxophilicity is based on the difference between the metal-oxygen and metal-sulfur bond dissociation enthalpies (BDEs), using a normalized scale that sets the oxophilicity of gold to 0 and that of hafnium to 1. A limitation of this oxophilicity scale is that it is not specific to the oxidation state of the metal, but rather is

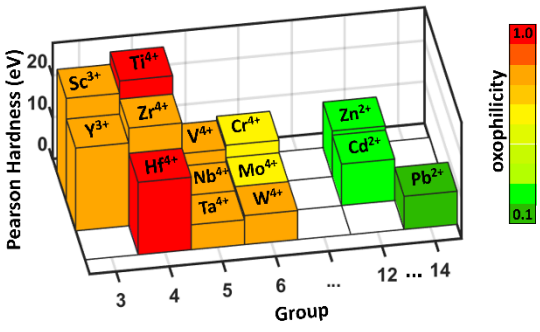

Figure 15. Graphical depiction of the Pearson hardness and oxophilicity (Kepp scale) of the transition metals discussed in this review, as well as the group 6 transition metals, Zn^{2+}, Cd^{2+}, and Pb^{2+}. The height of each bar corresponds to the Pearson hardness value in eV, and the bars are color-coded by oxophilicity according to the scale given at right (each color gradation represents a step of 0.1).

based on the BDEs of the species MO, MS, MO^+, and/or MS^+, using experimental values where available or computed values if not.

While neither of these scales (hardness and oxophilicity) perfectly captures the reactivity of the transition metals with respect to the synthesis of chalcogenide and oxide nanomaterials, a qualitative consideration of the two together predicts well some of the difficulties encountered in the preparation of chalcogenide materials. For example, both hardness and oxophilicity reach a maximum overall for the group 4 ions (Ti^{4+}, Zr^{4+}, and Hf^{4+}), helping to explain why the synthesis of the binary and ternary chalcogenides of these materials seems to require the most stringent conditions, usually including a lack of oxygen-bearing solvents and ligands. The group 3 trications Sc^{3+} and Y^{3+} are only slightly less oxophilic and softer, and the synthesis of $NaYS_2$ similarly required relatively harsh conditions, although it tolerated the use of oxygen-containing acetylacetonate and oleate precursors.

In moving to group 5 (V^{4+}, Nb^{4+}, and Ta^{4+}), despite similar oxophilicity values, a steep drop in Pearson hardness could help explain why there are many more known syntheses of chalcogenides of these ions, and they tolerate the presence of a wider range of ligands and precursors, including the use of oxide precursors such as vanadyl acetylacetonate and the use of oleic acid or oleyl alcohol as co-solvents.

Although not discussed in this review, the group 6 tetravalent cations (Cr^{4+}, Mo^{4+}, and W^{4+}) as well as Zn^{2+}, Cd^{2+}, and Pb^{2+} are included for comparison. While the Pearson hardness values for these ions level off at similar values as compared to group 5, there is a small drop in oxophilicity for group 6 and a major drop upon reaching Zn^{2+}, Cd^{2+}, and Pb^{2+}. Of course, these latter thiophilic ions make up some of the most ubiquitous chalcogenide nanomaterials known (CdS, ZnS, PbS, and the analogous selenium- and tellurium-containing congeners).[88]

This discussion is intended to illustrate two major points. First, as our survey earlier in this article shows, the synthesis of early transition metal chalcogenide colloidal nanomaterials is much less well-developed than that of the late transition metals and p-block metals, and the different properties of these ions dictates that as researchers seek to improve methodologies to access these materials, it will be necessary and desirable to design fundamentally new approaches and precursors in order to realize the same level of control in this part of the periodic table. Second, even within the early transition metals, the group 4 metals pose a particularly severe challenge, which is increasingly urgent to overcome given the exciting predicted properties of some of the group 4 chalcogenides, especially ternary chalcogenides such as the chalcogenide perovskites.

Focusing therefore on the ternary group 4 metal sulfides ($BaTiS_3$ and $BaZrS_3$, although the discussion is also relevant to related materials) we can briefly consider some of the chemical and mechanistic considerations that may contribute to the success of the protocols described earlier in producing colloidal nanocrystals of these materials. The choice of solvents, precursors, and reaction conditions are all critical, and we highlight opportunities to further develop in these areas.

Solvents and nanocrystal ligands: The choice of reaction solvent is limited by boiling point, stability/decomposition, precursor solubility, and coordinating ability. Early transition metal sulfides tend to require particularly high reaction temperatures to crystallize successfully, which generally limits the solvent choice to those with boiling points greater than 300 °C and sometimes higher. In most cases, the solvent(s) also functions as a surfactant which helps direct growth, and as ligands on the final particles to prevent aggregation and allow for stable colloidal dispersions to form, although mixtures of "inert" non-coordinating solvents and coordinating ligands can also be used.[89] The solvent must therefore have a strong enough coordinating ability to stabilize the particles against uncontrolled aggregation (which would tend to lead to the formation of "bulk" material rather than nanocrystals), but also must not bind so strongly that it renders the metal ion precursors unreactive. Notably, the reported syntheses of binary and ternary colloidal group 4 transition metal sulfides have almost universally used oleylamine as the only solvent, surfactant, and long-chain ligand, which suggests that this is an important area for further development to widen the synthetic landscape and provide better synthetic control over the nanomaterials in terms of shape, size, and dispersability.

Both of the reported solution-phase syntheses of $BaZrS_3$ nanocrystals have noted issues with aggregation, suggesting that oleylamine alone is inadequate to stabilize the surface of these materials, presumably due to its relatively weak binding ability towards the metal ions.[3,4] To further develop these materials, it will be necessary to identify other (preferably non-oxygen-containing) ligands that can be incorporated, perhaps as co-additives, such as chelating amines and dithiocarboxylates. The possible decomposition pathways of the ligand must also be considered; even oleylamine can decompose to produce metal nitrides under some circumstances.[90] The use of solvents with saturated carbon chains, which tend to be more stable with respect to decomposition, and ligands with higher boiling points, should also be considered.[91]

Precursors: Several key factors must be considered in precursor design and selection for early transition metal chalcogenide nanomaterial synthesis, including solubility, reactivity, and decomposition pathways and byproducts. Because the solvents must in general be weakly-coordinating (*vide supra*), the selection of precursors that will be soluble in these nonpolar, highly lipophilic, weakly coordinating solvents is a significant constraint. While the group 4 metal chlorides $TiCl_4$, $ZrCl_4$, and $HfCl_4$ are sufficiently soluble in oleylamine to be used as precursors for the binary chalcogenides, they have not proven to be suitable precursors for $BaTiS_3$ and $BaZrS_3$, possibly because they can lead to the formation of insoluble barium chloride *in situ*.[4] Instead, molecular homoleptic metal amides and metal dithiocarbamates bearing alkyl substituents, which help engender good solubility in nonpolar solvents, have been selected for these syntheses.

The sulfur precursors used in the synthesis of group 4 transition metal sulfide nanomaterials (CS_2, dialkyldithiocarbamate, and N,N'-diethylthiourea) are all believed to decompose *in situ* in oleylamine solution to generate the hydrogen sulfide anion (HS^-). Especially under basic conditions in amine solution, this serves as a suitably reactive source of sulfide anion to be able to lead to the formation of metal sulfides, even given the relatively weak metal-sulfur bonds formed by some of these elements. Figure 16 illustrates possible reaction pathways for the transformation of metal dithiocarbamates (Figure 16A) or metal amides in combination with diethylthiourea (Figure 16B) into metal hydrosulfides as an initial step in the

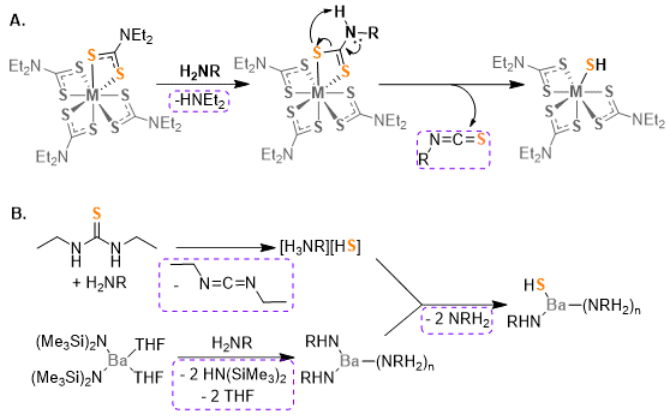

Figure 16. Plausible mechanisms for the initial steps in the formations of metal-sulfide monomers *en route* to $BaZrS_3$ or $BaTiS_3$ nanocrystals. Byproducts of the precursor transformation reactions are outlined in purple. H_2NR = oleylamine. (A) Reaction of a metal(IV) tetrakis(dithiocarbamate) complex with oleylamine first undergoes transamidation followed by decomposition to release a hydrosulfide ion which can bind to the metal. (B) Decomposition of N,N'-diethylthiourea in the presence of oleylamine generates a hydrosulfide ion; meanwhile, a barium bis(amide) precursor undergoes ligand exchange with oleylamine. The hydrosulfide ion can then bind to the barium ion concomitant with protonolysis of one of the oleylamide ligands.

formation of reactive monomers. The decomposition pathways of metal dithiocarbamates in oleylamine has been studied on late transition metals, and there is strong evidence that transamination with oleylamine occurs prior to decomposition, ultimately resulting in elimination of an alkyl isothiocyanate.[38,92] While this has not been studied on early transition metals, it seems likely that a qualitatively similar pathway is operative; this would be a useful avenue for further study. On the other hand, the decomposition of dialkylthioureas in organic amine solution has not been studied in detail mechanistically, therefore the pathway shown in Figure 16B is speculative, although it is based on theoretical calculations for the solid-state decomposition of thiourea.[93] The alkylammonium hydrosulfide species resulting from this decomposition could substitute for one of the metal amide ligands to produce a metal-sulfur bond.

An important feature of the sulfur and metal ion precursors in these reactions is that, upon decomposition or reaction, they give rise to byproducts which are not likely to strongly coordinate to the metal centers, and therefore do not compete with the formation of the metal sulfide material; this is illustrated in Figure 16 with the eliminated byproducts outlined. Any ligands or precursors which could decompose to give rise to oxides or oxide-containing species must most likely be avoided, and even precursors that release halide ions upon reaction can be problematic as noted above.

Given all these considerations, the scope of precursors for the group 4 transition metals remains fairly limited, especially for the formation of ternary species where the reactivity, solubility, and mutual interactions of multiple metal precursors must be considered. New precursors such as metal thiolates and metal dithiocarboxylates (some of which have already been applied in thin-film preparation by Bart and Agrawal)[40,46] or metal sulfide clusters could be considered. Sulfur- and selenium-containing complexes which have previously been used for chemical vapor deposition (CVD) of thin films provide another collection of possible single-source-precursor complexes. For example, group 4 (M = Ti, Zr, Hf) bis(cyclopentadienyl)-bis(selenolate) complexes have successfully served as CVD precursors for $TiSe_2$, $HfSe_2$, and $ZrSe_2$ thin films.[94] Additionally, thioether and selenoether complexes of the group 4 and 5 metals have previously been applied in the preparation of TiS_2, $TiSe_2$, NbS_2, $NbSe_2$, and VSe_2 thin films by CVD.[95–98] These compounds likely all have suitable solubility and reactivity properties for testing as single-source precursors in colloidal nanocrystal preparation.[99]

Reaction conditions: Compared to other classes of nanomaterials such as cadmium or lead chalcogenides and halide perovskites, early transition metal sulfides seem to generally require higher temperatures to successfully form nanocrystalline materials; this seems to be limited not necessarily by the reactivity of the precursors, but by the high temperatures needed to achieve crystallinity, since in some cases it has been shown or speculated that amorphous materials of a similar composition form at lower temperatures. In the case of $BaZrS_3$, the temperature may have a significant impact on the structure (*vide supra*), and the use of higher-boiling solvents or reaction set-ups that allow for pressurization could give rise to improved material quality. Furthermore, both reported syntheses of $BaZrS_3$ to date have relied on a heat-up approach, but a hot-injection approach may provide better control over morphology, as was observed for $BaTiS_3$, and should be pursued in the future; a hot-injection approach is feasible in principle even with single-source precursors.[100]

Size and morphological control: In some of the examples discussed here, researchers have been able to demonstrate a degree of control over the size and morphology of colloidally-prepared nanoparticles. Size can often be tuned by altering the reaction time and/or temperature, with an increase in either giving rise to larger particles in the cases studied here (see Table S1). The factors involved in changing particle shape and morphology can be complex, but are generally understood to arise at least in part from the relative binding affinities of ligands and monomers to different facets of the growing nanocrystal; therefore, altering ligands and solvents is a common tactic for tuning morphology. Unfortunately, as noted above, the choice of solvents and ligands for these early transition metal chalcogenides, especially for the group 4 metals, is currently limited, which also hinders the development of morphological control. As a wider library of solvents, ligands, and precursors are developed, it is likely that better control over a wider range of particle shapes and sizes will also ensue. An improved understanding of the surface chemistry of the particles will help in rationally targeting different morphologies. Interestingly, other subtle factors can also have a major effect on particle size and shape; for example, we found that for $BaTiS_3$ nanorods prepared by hot injection, the aspect ratio of the nanorods could be tuned from 1.4:1 to 10:1 simply by changing the concentration of the reaction mixture.[33] However, the reason for this is not well understood and is a subject of future investigation.

Reproducibility, yield, and scalability: Reproducibility, yield, and scalability are additional issues that must be addressed in the long term as improved syntheses of early transition metal chalcogenide nanomaterials are developed. Scalability is a common issue with colloidal nanocrystal synthesis in general; although not necessarily critical for fundamental research, the ability to readily produce large quantities of material may be important for certain potential applications. Some synthetic approaches are more inherently

scalable than others—for example, heat-up approaches may in general be easier to carry out on a large scale than hot-injection approaches, although some methods for upscaling hot-injection syntheses have been developed.[101] These issues should be taken into consideration in reaction development when scalability is an ultimate goal. For most of the examples discussed herein, the scale of the reaction is on the order of 1 mmol or less, although in a few cases scale-up to the gram scale (e.g., 40 mmol for VSe_2) was described.[57,59] Unfortunately, reaction yields are infrequently reported in descriptions of nanocrystal syntheses; however, when given, mass yields for the reactions described here are mostly moderate to good (~40-80%).[31,57,59,67] For example, we reported a yield of approximately 48% for the synthesis of $BaZrS_3$ nanocrystals.[3] Although there is room for improvement, this suggests that reaction yield may not be an inherently limiting factor in the development of early transition metal chalcogenide nanomaterial synthesis.

It can be challenging to achieve a high degree of reproducibility (in terms of material identity, purity, size, morphology, and properties) in nanocrystal synthesis.[102] In the discussion above, we mentioned a few cases where similar reaction conditions seemed to give rise to slightly different material outcomes; however, since different research groups rarely employ the exact same reaction conditions and work-up procedures, direct comparisons can be difficult, and published reports rarely explicitly comment on the reproducibility of the results. Properties such as particle morphology and aggregation behavior can be highly dependent on minor changes to the reaction conditions (such as heating or cooling rate, purity of starting materials, the temperatures and pressures used for drying and degassing steps, and details of the workup procedure), as some of the reports discussed above have highlighted.[63,72]

Although some of the early transition metal chalcogenide materials discussed here have been reported in the literature by a number of different research groups, there are some whose colloidal synthesis has only been reported by one research group, especially for the group 3-4 transition metals. These include $TiSe_2$, ZrS_2, $ZrSe_3$, HfS_2, and $HfSe_3$, for which the solution-phase nanocrystal synthesis from molecular precursors has only been unambiguously reported by the Cheon group;[21,29,31] $NaYS_2$, which has been reported by Zhang and Yan;[20] and $BaTiS_3$, which has only been reported by us.[33,37] Therefore, the question of whether these syntheses will prove reproducible in the hands of other researchers remains open.

Conclusion and Outlook

The field of solution-phase synthesis of early transition metal (groups 3-5) chalcogenide nanomaterials is still in its infancy, despite rapid growth in the last few years. Looking back over the examples described in this paper, one can see qualitative evidence for this in that fact that only a small handful of these nanomaterials were reported before 2012, and the majority of the syntheses described here were reported in 2020 or later. Even for some simple binary materials, only a few examples have been described, and control over size and morphology is often poor. Overall, very few ternary materials in this class have been studied, although interest in the chalcogenide perovskites and related materials is likely to drive considerable focused efforts in this area in the immediate future. Of the syntheses that have been reported, only rarely has a systematic study of reaction parameters (such as concentration, stoichiometry, temperature, solvent, co-ligands, etc) been reported, and little mechanistic information is available about precursor conversion. There have been essentially no studies about the nature of the surfaces and surface-ligand interactions in these materials, which could differ significantly from those known in the more well-studied late-metal chalcogenides. These areas, along with others described in the previous section, represent important needs for future investigations. We hope, therefore, for this article to serve as a useful *early-stage* account of this field from a synthetic point of view, to help those interested in this class of materials to understand the current state-of-the-art and the areas where further development and innovation is needed.

Author Contributions

DZ: Writing – Original Draft, Writing – Review & Editing. SEC: Writing—Original Draft, Writing—Review & Editing, Supervision, Funding Acquisition.

Conflicts of interest

There are no conflicts of interest to declare.

Acknowledgements

This work was supported by the National Science Foundation of the United States (Grant #2004421 and Grant #2237082).

Notes and references

1 K. V. Sopiha, C. Comparotto, J. A. Márquez and J. J. S. Scragg, *Adv. Opt. Mater.*, 2022, **10**, 2101704.
2 V. K. Ravi, S. H. Yu, P. K. Rajput, C. Nayak, D. Bhattacharyya, D. S. Chung and A. Nag, *Nanoscale*, 2021, **13**, 1616–1623.
3 D. Zilevu, O. O. Parks and S. E. Creutz, *Chem. Commun.*, 2022, **58**, 10512–10515.
4 R. Yang, A. D. Jess, C. Fai and C. J. Hages, *J. Am. Chem. Soc.*, 2022, **144**, 15928–15931.
5 A. B. Kehoe, D. O. Scanlon and G. W. Watson, *J. Phys. Condens. Matter*, 2016, **28**, 175801.
6 R. Prado-Rivera, C.-Y. Chang, M. Liu, C.-Y. Lai and D. R. Radu, *Nanomaterials*, 2021, **11**, 823.
7 A. B. Kehoe, D. O. Scanlon and G. W. Watson, *J. Mater. Chem. C*, 2015, **3**, 12236–12244.
8 L. Wang, M. Jiang, F. Liu, Q. Huang, L. Liu, L. Fu and Y. Wu, *Energy Fuels*, 2020, **34**, 11590–11596.
9 S. Kim, Y. J. Kim and W.-H. Ryu, *Appl. Surf. Sci.*, 2021, **547**, 149029.
10 Y.-Y. Liu, L. Xu, X.-T. Guo, T.-T. Lv and H. Pang, *J. Mater. Chem. A*, 2020, **8**, 20781–20802.
11 Y. Liu, J. Wu, K. P. Hackenberg, J. Zhang, Y. M. Wang, Y. Yang, K. Keyshar, J. Gu, T. Ogitsu, R. Vajtai, J. Lou, P. M. Ajayan, B. C. Wood and B. I. Yakobson, *Nat. Energy*, 2017, **2**, 1–7.
12 L. Najafi, S. Bellani, R. Oropesa-Nuñez, B. Martín-García, M. Prato, L. Pasquale, J.-K. Panda, P. Marvan, Z. Sofer and F. Bonaccorso, *ACS Catal.*, 2020, **10**, 3313–3325.

13 T. Das, S. Chakraborty, R. Ahuja and G. P. Das, *ChemPhysChem*, 2019, **20**, 608–617.
14 J. H. Han, M. Kwak, Y. Kim and J. Cheon, *Chem. Rev.*, 2018, **118**, 6151–6188.
15 A. Giri, G. Park and U. Jeong, *Chem. Rev.*, 2023, **123**, 3329–3442.
16 M. Nasilowski, B. Mahler, E. Lhuillier, S. Ithurria and B. Dubertret, *Chem. Rev.*, 2016, **116**, 10934–10982.
17 R. Atif, A. Zarkov, D. R. C. Asuigui, P. Glaser, O. Stewart and S. L. Stoll, *Chem. Mater.*, 2019, **31**, 7779–7789.
18 J. Gu, Z.-Q. Zhao, Y. Ding, H.-L. Chen, Y.-W. Zhang and C.-H. Yan, *J. Am. Chem. Soc.*, 2013, **135**, 8363–8371.
19 G. Gouget, M. Pellerin, R. Al Rahal Al Orabi, L. Pautrot-D'Alençon, T. Le Mercier and C. B. Murray, *J. Am. Chem. Soc.*, 2021, **143**, 3300–3305.
20 Y. Ding, J. Gu, T. Zhang, A.-X. Yin, L. Yang, Y.-W. Zhang and C.-H. Yan, *J. Am. Chem. Soc.*, 2012, **134**, 3255–3264.
21 D. Yoo, M. Kim, S. Jeong, J. Han and J. Cheon, *J. Am. Chem. Soc.*, 2014, **136**, 14670–14673.
22 J. van Embden, A. S. R. Chesman and J. J. Jasieniak, *Chem. Mater.*, 2015, **27**, 2246–2285.
23 S. G. Kwon and T. Hyeon, *Small*, 2011, **7**, 2685–2702.
24 K. H. Park, J. Choi, H. J. Kim, D.-H. Oh, J. R. Ahn and S. U. Son, *Small*, 2008, **4**, 945–950.
25 V. V. Plashnitsa, F. Vietmeyer, N. Petchsang, P. Tongying, T. H. Kosel and M. Kuno, *J. Phys. Chem. Lett.*, 2012, **3**, 1554–1558.
26 C. de Mello Donegá, P. Liljeroth and D. Vanmaekelbergh, *Small*, 2005, **1**, 1152–1162.
27 S. Prabakar, C. W. Bumby and R. D. Tilley, *Chem. Mater.*, 2009, **21**, 1725–1730.
28 S. Prabakar, S. Collins, B. Northover and R. D. Tilley, *Chem. Commun.*, 2010, **47**, 439–441.
29 S. Jeong, D. Yoo, J. Jang, M. Kim and J. Cheon, *J. Am. Chem. Soc.*, 2012, **134**, 18233–18236.
30 S. Jeong, J. H. Han, J. Jang, J. Seo, J.-G. Kim and J. Cheon, *J. Am. Chem. Soc.*, 2011, **133**, 14500–14503.
31 J. Jang, S. Jeong, J. Seo, M.-C. Kim, E. Sim, Y. Oh, S. Nam, B. Park and J. Cheon, *J. Am. Chem. Soc.*, 2011, **133**, 7636–7639.
32 P. Fadojutimi, Z. Tetana, J. Moma, N. Moloto and S. Gqoba, *ChemistrySelect*, 2022, **7**, e202202293.
33 D. Zilevu and S. E. Creutz, *Chem. Mater.*, 2021, **33**, 5137–5146.
34 M. P. Hendricks, M. P. Campos, G. T. Cleveland, I. Jen-La Plante and J. S. Owen, *Science*, 2015, **348**, 1226–1230.
35 M. Saeki, M. Onoda and Y. Yajima, *J. Solid State Chem.*, 1996, **121**, 451–456.
36 M. Saeki and M. Onoda, *J. Solid State Chem.*, 1993, **102**, 100–105.
37 N. E. Ingram, B. J. Jordan, B. Donnadieu and S. E. Creutz, *Dalton Trans.*, 2021, **50**, 15978–15982.
38 J. C. Sarker and G. Hogarth, *Chem. Rev.*, 2021, **121**, 6057–6123.
39 A. C. Behrle, A. J. Myers, A. Kerridge and J. R. Walensky, *Inorg. Chem.*, 2018, **57**, 10518–10524.
40 J. W. Turnley, K. C. Vincent, A. A. Pradhan, I. Panicker, R. Swope, M. C. Uible, S. C. Bart and R. Agrawal, *J. Am. Chem. Soc.*, 2022, **144**, 18234–18239.
41 A. Clearfield, *Acta Crystallogr.*, 1963, **16**, 135–142.
42 R. Lelieveld and D. J. W. IJdo, *Acta Crystallogr. B*, 1980, **36**, 2223–2226.
43 S. Niu, B. Zhao, K. Ye, E. Bianco, J. Zhou, M. E. McConney, C. Settens, R. Haiges, R. Jaramillo and J. Ravichandran, *J. Mater. Res.*, 2019, **34**, 3819–3826.
44 H. Hahn and U. Mutschke, *Z. Für Anorg. Allg. Chem.*, 1957, **288**, 269–278.
45 C. Comparotto, A. Davydova, T. Ericson, L. Riekehr, M. V. Moro, T. Kubart and J. Scragg, *ACS Appl. Energy Mater.*, 2020, **3**, 2762–2770.
46 A. A. Pradhan, M. C. Uible, S. Agarwal, J. W. Turnley, S. Khandelwal, J. M. Peterson, D. D. Blach, R. N. Swope, L. Huang, S. C. Bart and R. Agrawal, *Angew. Chem. Int. Ed.*, 2023, **62**, e202301049.
47 K. Xu, P. Chen, X. Li, C. Wu, Y. Guo, J. Zhao, X. Wu and Y. Xie, *Angew. Chem. Int. Ed.*, 2013, **52**, 10477–10481.
48 H. Lin, S. He, Z. Mao, J. Miao, M. Xu and Q. Li, *Nanotechnology*, 2017, **28**, 445603.
49 Q. Zhu, M. Shao, S. H. Yu, X. Wang, Z. Tang, B. Chen, H. Cheng, Z. Lu, D. Chua and H. Pan, *ACS Appl. Energy Mater.*, 2019, **2**, 644–653.
50 L. Wang, Z. Wu, M. Jiang, J. Lu, Q. Huang, Y. Zhang, L. Fu, M. Wu and Y. Wu, *J. Mater. Chem. A*, 2020, **8**, 9313–9321.
51 K. L. Salvatore, S. Tan, C. Tang, J. Gan, M. Licht, C.-H. Lin, X. Tong, Y. K. Chen-Wiegart, E. S. Takeuchi, K. J. Takeuchi, A. C. Marschilok and S. S. Wong, *ACS Sustain. Chem. Eng.*, 2020, **8**, 16397–16412.
52 B. Liu, L. Wang, Y. Zhu, H. Peng, C. Du, X. Yang, Q. Zhao, J. Hou and C. Cao, *ACS Nano*, 2022, **16**, 12900–12909.
53 G. Lui, G. Jiang, A. Duan, J. Broughton, J. Zhang, M. W. Fowler and A. Yu, *Ind. Eng. Chem. Res.*, 2015, **54**, 2682–2689.
54 J. Zhou, L. Wang, M. Yang, J. Wu, F. Chen, W. Huang, N. Han, H. Ye, F. Zhao, Y. Li and Y. Li, *Adv. Mater.*, 2017, **29**, 1702061.
55 F. Ming, H. Liang, Y. Lei, W. Zhang and H. N. Alshareef, *Nano Energy*, 2018, **53**, 11–16.
56 Q. Jiang, J. Wang, Y. Jiang, L. Li, X. Cao and M. Cao, *Nanoscale*, 2020, **12**, 8858–8866.
57 W. Zhao, B. Dong, Z. Guo, G. Su, R. Gao, W. Wang and L. Cao, *Chem. Commun.*, 2016, **52**, 9228–9231.
58 Z. Guo, L. Yang, W. Wang, L. Cao and B. Dong, *J. Mater. Chem. A*, 2018, **6**, 14681–14688.
59 W. Feng, M. Cheng, R. Du, Y. Wang, P. Wang, H. Li, L. Song, X. Wen, J. Yang, X. Li, J. He and J. Shi, *Adv. Mater. Interfaces*, 2022, **9**, 2200060.
60 M. Liu, C.-Y. Lai, M. Zhang and D. R. Radu, *Sci. Rep.*, 2020, **10**, 21679.
61 J. Zhang, J. Li, H. Huang, W. Chen, Y. Cui, Y. Li, W. Mao, X. Zhu and X. Li, *Small*, 2022, **18**, 2204557.
62 R. L. Brutchey, *Acc. Chem. Res.*, 2015, **48**, 2918–2926.
63 P. Sekar, E. C. Greyson, J. E. Barton and T. W. Odom, *J. Am. Chem. Soc.*, 2005, **127**, 2054–2055.
64 J. Guo, Y. Shi, C. Zhu, L. Wang, N. Wang and T. Ma, *J. Mater. Chem. A*, 2013, **1**, 11874–11879.
65 C.-Y. Chang, R. Prado-Rivera, M. Liu, C.-Y. Lai and D. R. Radu, *ACS Nanosci. Au*, 2022, **2**, 440–447.
66 T. Kolokoto, V. Mashindi, R. Kadzutu-Sithole, L. F. E. Machogo-Phao, Z. B. Ndala, N. P. Shumbula, S. S. Nkabinde, G. N. Ngubeni, S. S. Gqoba, K. P. Mubiayi and N. Moloto, *RSC Adv.*, 2021, **11**, 31159–31173.
67 T. Y. Kim, C. Woo, K. H. Choi, X. Dong, J. Jeon, J. Ahn, X. Zhang, J. Kang, H.-S. Oh, H. K. Yu and J.-Y. Choi, *Nanoscale*, 2022, **14**, 17365–17371.
68 J. Zhang, C. Du, Z. Dai, W. Chen, Y. Zheng, B. Li, Y. Zong, X. Wang, J. Zhu and Q. Yan, *ACS Nano*, 2017, **11**, 10599–10607.
69 A. Mansouri and N. Semagina, *ACS Appl. Nano Mater.*, 2018, **1**, 4408–4412.
70 W. Li, X. Wei, H. Dong, Y. Ou, S. Xiao, Y. Yang, P. Xiao and Y. Zhang, *Front. Chem.*, 2020, **8**, 189.
71 C. L. Stender, P. Sekar and T. W. Odom, *J. Solid State Chem.*, 2008, **181**, 1621–1627.
72 W. Shen, L. Qiao, J. Ding and Y. Sui, *J. Alloys Compd.*, 2023, **935**, 167877.
73 M. Liu, C.-Y. Lai, C.-Y. Chang and D. R. Radu, *Crystals*, 2021, **11**, 51.
74 C.-C. Chen, K. H. Stone, C.-Y. Lai, K. D. Dobson and D. Radu, *Mater. Lett.*, 2018, **211**, 179–182.
75 V. Mantella, S. Ninova, S. Saris, A. Loiudice, U. Aschauer and R. Buonsanti, *Chem. Mater.*, 2019, **31**, 532–540.

76 M. Liu, C.-Y. Lai, G. S. Selopal and D. R. Radu, *PLOS ONE*, 2020, **15**, e0232184.
77 Y. Zhao, M. Liu, W. Zhang, X. Sun, W. Wang, W. Zhang, M. Tang, W. Ren, M. Sun, W. Feng and W. Wang, *Dalton Trans.*, 2022, **51**, 16937–16944.
78 A. Haque, S. Ershadrad, T. D. Chonamada, D. Saha, B. Sanyal and P. K. Santra, *J. Mater. Chem. A*, 2022, **10**, 19925–19934.
79 X. Wu, B. Wu, H. Wang, Q. Zhuang, Z. Xiong, H. Yi, P. Xu, G. Shi, Y. Guo and B. Wang, *Energy Fuels*, 2021, **35**, 11563–11571.
80 Y. Liu, T. Ding, X. Luo, Y. Li, J. Long and K. Wu, *Chem. Mater.*, 2020, **32**, 224–233.
81 J. H. Han, S. Lee, D. Yoo, J.-H. Lee, S. Jeong, J.-G. Kim and J. Cheon, *J. Am. Chem. Soc.*, 2013, **135**, 3736–3739.
82 H. Wang, X. Huang, J. Lin, J. Cui, Y. Chen, C. Zhu, F. Liu, Q. Zeng, J. Zhou, P. Yu, X. Wang, H. He, S. H. Tsang, W. Gao, K. Suenaga, F. Ma, C. Yang, L. Lu, T. Yu, E. H. T. Teo, G. Liu and Z. Liu, *Nat. Commun.*, 2017, **8**, 394.
83 S. Nagata, T. Aochi, T. Abe, S. Ebisu, T. Hagino, Y. Seki and K. Tsutsumi, *J. Phys. Chem. Solids*, 1992, **53**, 1259–1263.
84 E. Navarro-Moratalla, J. O. Island, S. Mañas-Valero, E. Pinilla-Cienfuegos, A. Castellanos-Gomez, J. Quereda, G. Rubio-Bollinger, L. Chirolli, J. A. Silva-Guillén, N. Agraït, G. A. Steele, F. Guinea, H. S. J. van der Zant and E. Coronado, *Nat. Commun.*, 2016, **7**, 11043.
85 K. P. Kepp, *Inorg. Chem.*, 2016, **55**, 9461–9470.
86 R. G. Pearson, *Inorg. Chem.*, 1988, **27**, 734–740.
87 A. Kramida, Y. Ralchenko, J. Reader, and NIST ASD Team, *NIST Atomic Spectra Database* (*ver. 5.10)*, http://physics.nist.gov/asd (accessed April 2023).
88 F. P. García de Arquer, D. V. Talapin, V. I. Klimov, Y. Arakawa, M. Bayer and E. H. Sargent, *Science*, 2021, **373**, eaaz8541.
89 A. Heuer-Jungemann, N. Feliu, I. Bakaimi, M. Hamaly, A. Alkilany, I. Chakraborty, A. Masood, M. F. Casula, A. Kostopoulou, E. Oh, K. Susumu, M. H. Stewart, I. L. Medintz, E. Stratakis, W. J. Parak and A. G. Kanaras, *Chem. Rev.*, 2019, **119**, 4819–4880.
90 M. Parvizian, A. Duràn Balsa, R. Pokratath, C. Kalha, S. Lee, D. Van den Eynden, M. Ibáñez, A. Regoutz and J. De Roo, *Angew. Chem. Int. Ed.*, 2022, **61**, e202207013.
91 B. M. Sperry, N. A. Kukhta, Y. Huang and C. K. Luscombe, *Chem. Mater.*, 2023, **35**, 570–583.
92 N. Hollingsworth, A. Roffey, H.-U. Islam, M. Mercy, A. Roldan, W. Bras, M. Wolthers, C. R. A. Catlow, G. Sankar, G. Hogarth and N. H. de Leeuw, *Chem. Mater.*, 2014, **26**, 6281–6292.
93 Z. D. Wang, M. Yoshida and B. George, *Comput. Theor. Chem.*, 2013, **1017**, 91–98.
94 A. L. Hector, W. Levason, G. Reid, S. D. Reid and M. Webster, *Chem. Mater.*, 2008, **20**, 5100–5106.
95 S. D. Reid, A. L. Hector, W. Levason, G. Reid, B. J. Waller and M. Webster, *Dalton Trans.*, 2007, 4769–4777.
96 A. L. Hector, M. Jura, W. Levason, S. D. Reid and G. Reid, *New J. Chem.*, 2009, **33**, 641–645.
97 S. L. Benjamin, Y.-P. Chang, C. Gurnani, A. L. Hector, M. Huggon, W. Levason and G. Reid, *Dalton Trans.*, 2014, **43**, 16640–16648.
98 S. L. Benjamin, C. H. (Kees) de Groot, C. Gurnani, A. L. Hector, R. Huang, K. Ignatyev, W. Levason, S. J. Pearce, F. Thomas and G. Reid, *Chem. Mater.*, 2013, **25**, 4719–4724.
99 S. Mishra, *Chem. Commun.*, 2022, **58**, 10136–10153.
100 Y. Zhao, F. T. Rabouw, T. van Puffelen, C. A. van Walree, D. R. Gamelin, C. de Mello Donegá and A. Meijerink, *J. Am. Chem. Soc.*, 2014, **136**, 16533–16543.
101 M. Yarema, O. Yarema, W. M. M. Lin, S. Volk, N. Yazdani, D. Bozyigit and V. Wood, *Chem. Mater.*, 2017, **29**, 796–803.
102 L. M. Liz-Marzán, C. R. Kagan and J. E. Millstone, *ACS Nano*, 2020, **14**, 6359–6361.